The Thesis Committee for Oguz Incedalip
Certifies that this is the approved version of the following thesis:

Thermal Modeling for Calculation of Formation Temperatures for Deep Water Wells with Chemical Heat Source

APPROVED BY
SUPERVISING COMMITTEE:

Supervisor:

Eric van Oort

David Nicolas Espinoza

Thermal Modeling for Calculation of Formation Temperatures for Deep Water Wells with Chemical Heat Source

by

Oguz Incedalip, B.S.

Thesis

Presented to the Faculty of the Graduate School of

The University of Texas at Austin

in Partial Fulfillment

of the Requirements

for the Degree of

Master of Science in Engineering

The University of Texas at Austin

December 2015

Dedication

To my family for their immense love and support.

Acknowledgements

First and foremost, I would like to thank my supervisor, Dr. Eric van Oort for giving me an opportunity to work in his research group which has been a great experience. His guidance, valuable feedback and encouragement are the most important factors for success of this thesis. I also wish to thank Dr. David Nicolas Espinoza for being co-reader of my thesis and providing expert technical advice and taking genuine interest in my project.

I wish to express my sincere thanks to Dr. Ali Karimi and Besmir Hoxha for helping me throughout the project and sharing their experience. Their support, motivation, assistance made this project possible. I would also like to thank Tesse Smitherman, Glen Baum, and Gary Miscoe for their technical and administrative support throughout my graduate study. It was a great pleasure to work with these wonderful people.

I would like to thank our sponsor Shell for their financial and technical support for this project. Particularly, I wish to thank Dr. Arthur Hale, Deandre Reagins, Dr. Qing Tang, and Dr. Anastasia Dobroskok for supplying invaluable information, and improving the project with positive input and support.

I would like to take this opportunity to thank my family and friends for believing in me and supporting me throughout this challenging process. I want to express my gratitude to my family for their unconditional love. Specifically, I would like to thank Eduardo Ramirez for being there whenever I needed. I cannot thank enough for his endless support and motivation. I would like to express my gratitude to each and every person who helped me directly or indirectly during this journey.

Abstract

Thermal Modeling for Calculation of Formation Temperatures for Deep Water Wells with Chemical Heat Source

Oguz Incedalip, M. S. E.

The University of Texas at Austin, 2015

Supervisor: Eric van Oort

Drilling through depleted zones is becoming more common as the resources are exhausted and the fields mature. To be able to access deeper sections of the reservoirs, it is essential to drill through depleted zones effectively. This need brings around the challenges including severe lost circulation and poor zonal isolation. Artificially strengthening the wellbore is of crucial importance in order to achieve successful drilling as well as cementing for deep water wells. Altering the thermal stresses results in increased tangential stresses in the vicinity of the wellbore and therefore increases the fracture gradient. Thermal stresses can be increased through a controlled exothermic chemical reaction of certain salts which are coated via pharmaceutical techniques to delay the reaction until the carrier fluid transports the materials to the target zone. This approach with its innovative method surpasses other methods like downhole heaters as it is more practically feasible. The technique has a great potential to decrease mud losses, hence to decrease non-productive cost and time.

In this study a computational thermal model is developed in order to calculate the temperature distribution of the formation as well as the annular and tubular fluids for

given heat generation rates. The numerical model which uses finite volume techniques is developed for an axisymmetric cylindrical geometry including the drilling fluid, casing, annulus, and formation for transient heat transfer including a time and location dependent heat generation source.

The results are analyzed in comparison to one analytical solution as well as a commercial software package, Drill Bench, in order to verify the accuracy of the model for scenarios with no heat generation, since modelling of heat generation is not available for the other approaches. Some parameters of the model such as the heat transfer coefficient are calibrated in order to achieve the best agreement between different analyses.

Heat generation rates are obtained for different chemical compounds tested in insulated calorimeter experiments. The results of different heat generation rates for different heat generation durations as well other problem parameters such as circulation rate are investigated. In addition, thermal stress calculations based on the temperature increase are also presented.

Table of Contents

List of Tables

List of Figures

Chapter 1: Introduction

In this chapter, the motivation behind this study was discussed. The need and potential use of calculating the near-wellbore temperature distribution and its implication on the thermal stresses were mentioned in this chapter. In addition, the prior work related to temperature calculation for drilling operations was presented.

1.1 Motivation and Objective

New oil and gas wells are becoming more and more challenging to drill as hydrocarbon resources are exhausted and the wells become deeper and more complicated. Depleted zones in off-shore drilling are becoming more common and more wells are drilled in mature fields in order to enhance the hydrocarbon recovery or to produce from deeper reservoirs below previously produced zones. Hence, in order to be able reach deeper sections of the reservoirs, drilling through depleted zones is inevitable. These kind of zones are generally either produced or producing reservoirs overlaid and interbedded with shale layers. Pressure overbalances are typically on the order of thousands of psi and sometimes as high as 13,000 psi as reported in Gulf of Mexico (Adachi et al. 2004).

Drilling through these zones is challenging as the operation pressure range becomes narrower, since the difference between pore pressure and facture pressure decreases. The effects of the change in fracture gradients on the drilling fluid characteristics to maintain wellbore stability changes. Because of the smaller tolerances in operating conditions, the impact of drilling parameters on downhole conditions becomes more crucial.

One of the most important challenges in drilling through depleted zones is wellbore stability. The presence of normally pressurized shales requires a high mud weight drilling sections containing depleted zones. Along with wellbore instability, lost

circulation is another major problem for depleted zones. The loss of drilling fluid into the fractures is costly. On average 10 – 20% of the entire cost of drilling a high pressure high temperature well comes from the lost drilling fluid according to the U.S Energy Department. Note that the estimated industry cost is $2 – $4 billion/year worldwide, $1 billion/year of which is invested Gulf of Mexico (Growcock, *How to Stabilize and Strengthen the Wellbore during Drilling Operations,* SPE Distinguished Lecturer Program). Lost circulation may cause well control issues as well as financial problems. Pre-existing and drilling induced fractures may cause loss of productivity. In addition, fractures may intensify the wellbore stability problem. Drilling through depleted zones presents challenging problems in terms of lost circulation as well as zonal isolation problems. Wellbore strengthening now becomes critically important for efficient and sustained production.

A novel thermo-mechanical method was already suggested for wellbore strengthening. The fracture gradient in the vicinity of the wellbore can be increased by increasing the thermal stress by altering the temperature distribution of the formation (Closmann & Focas, 1978). Although the idea was suggested by Closmann and Focas a couple of decades ago, it is still challenging to find efficient methods to increase the formation temperature, especially for deeper wells. Heat sources including electrical, electromagnetic, or chemical have been suggested by various authors (Bohun 2000, Parman 2014, Jamaluddin 1998).

In this study, a chemical heat source was investigated to increase the near wellbore temperature and thermal stresses. An exothermic chemical reaction can be utilized to generate sufficient heat in the wellbore to manipulate the temperature distribution of the formation. The candidate chemical reactions were chosen by considering the compatibility of the reaction and the products of the reaction with the

regular drilling operation, stability of the formation, environmental considerations and legal regulations. In that sense the chemical reaction was chosen to be controllable and easy to handle, so that the method can be applied efficiently and safely in the field.

Dissolutions of certain chemical compounds in the water may generate high amounts of heat, resulting in desired temperature increases in the formation. Throughout this study, various chemical compounds were evaluated based on their heat generation potential and the effects of the compound to the regular drilling operations and procedures. Primary focus is also on the drilling fluid properties after the chemical reaction.

The laboratory studies on the delivery method of the chemically reactive compounds to the desired location consists of two parts: (1) delaying the reaction until the materials are carried to the desired location by the carrier fluid, (2) designing the carrier fluid. Pharmaceutical methods were utilized to coat the particles so that the coated actual particles are insoluble in the carrier fluid until they reach the target zone. Thus the reaction is delayed for a specified time, which can be controlled via coating thickness and properties. The carrier fluid was designed in such a way that the effect of the materials other than the water in the fluid on the reaction kinetics was minimal. Regular mud checks were also done to verify that the carrier fluid meets drilling operation requirements.

In order to be able to estimate the effects of this heat generation process in terms of temperature distribution in the formation, as well as the drilling fluid temperature in the wellbore, a heat transfer model was needed. Since analytical methods are not sufficient to model a complex system like this, a numerical method needed to be developed. Although there have been many studies suggesting analytical as well as numerical methods to investigate the temperature distribution during drilling operations,

a comprehensive model including both drilling fluid and formation temperatures, and time dependent heat generation term was not yet available. The purpose of this study was to develop a numerical model, including wellbore and the formation in the close vicinity of the wellbore, to calculate the transient temperature distribution based on experimental data for of generation rates of different chemical reactions. The temperature increase data at various locations within the formation was then used to calculate the thermal stresses.

This thesis is divided into 5 chapters. This chapter presents the introduction, and reviews the previous studies related to this work.

Chapter 2 explains the mathematical and numerical background of the developed method.

Chapter 3 presents a comparison with two other methods to evaluate the results of the new model.

Chapter 4 presents the results of various different chemical compounds and different operating conditions. The experimental procedures are explained in this chapter along with the thermal stress calculations based on the temperature distribution calculation.

Chapter 5 concludes this thesis and provides some ideas for further study in the subject.

1.2 Literature Review

Ramey (Ramey, JR 1962) developed an analytical model for the wellbore heat transfer problem involved in hot or cold fluid injections. The method estimates the temperature distributions of the fluids, tubing and casing as a function time and depth. The solution method assumes that the heat transfer within the wellbore is steady state, whereas the heat transfer to –or from– the formation is transient. The heat transfer within

the formation is assumed to be time dependent radial conduction, i.e., the heat transfer in the axial direction is omitted. The reliability of the solution methods is verified by comparing the computed results to the field results.

Edwardson (Edwardson et al. 1962) suggested another analytical model to calculate the changes in the formation temperature due to circulation of drilling fluids in order to be able to interpret electric logs quantitatively. This requires knowledge of formation temperature. The model is based on the solutions of the differential equations for heat conduction. Edwardson used field data to verify the computed formation temperatures.

Raymond (Raymond 1969) developed an analytical model with the motivation to predict mud properties at downhole conditions as the wells become deeper and hotter. He calculated drilling temperature via a pseudo-steady state solution, although he concluded that all the temperatures in the circulation system changes with time, never reaching steady state. He proved that the maximum fluid temperature occurs at one-fourth to one-third of the way up in the annulus.

Holmes (Holmes and Swift 1970) developed an analytical mathematical model that could be used to predict the mud temperature in the drill pipe and annulus while drilling at any depth in the well. This modeling was a solution of the steady-state equation for the heat transfer between the fluids in the annulus and the fluids in the drill pipe. The model was based upon the assumption that the heat transfer between the annular fluid and the formation could be approximated by steady-state linear heat transfer, since the heat transfer between the annular and tubular fluids is much larger than the heat transfer with the formation (due to relatively low thermal conductivity of the formation and the film resistance at the interface of mud and the rock). Based on the

Edwardson's work (Edwardson et al. 1962), it can be concluded that the temperature was relatively constant at any point sufficiently removed from the drill bit. This effect showed that the steady-state assumption appeared to be a close enough approximation of this phenomenon. Other simplifying assumptions were that the heat generated by the drill bit was considered negligible and that a linear geothermal profile exists.

Schoeppel (Schoeppel and Bennett 1971) developed a numerical simulation of borehole and formation temperature distributions. The method was used to model numerically the non-steady state temperature distributions in a circulating drilling fluid and the surrounding formation. The model includes the conduction and the forced convection within the drilling fluid and the adjacent formation using fourth order partial differential equations, which are solved using finite difference techniques with implicit time algorithms. Computer simulation time for solution of the numerical model was reasonably short. The method was found to provide an accurate solution to the problem of predicting non-steady state temperature distributions associated with drilling of a well.

Wooley (Wooley 1980) presented a model for predicting downhole wellbore temperatures in flowing or shut-in fluid streams, in casing and cement, and in formations. Flowing options include injection/production, forward/reverse circulation, and drilling. Model predictions agree with field temperature data. The influences of temperature, flow rate, and depth on downhole temperatures were presented.

Marshall (Marshall and Lie 1992) provided a finite difference approach, simultaneously solving all the heat transfer equations. Predictions of bottom hole and return temperatures from this model were shown to closely agree with the available field data.

Brown (Brown, Clapham et al. 1996) developed a transient heat transfer model in pipeline bundles. The model was coupled to the transient, multiphase flow simulator

OLGA. The lines containing the multiphase production fluids were modeled by OLGA, and the heat transfer between the internal lines, carrier pipe, and surroundings was handled by the bundle model. The model had been applied extensively to the design of a subsea, heated bundle system for the Britannia gas condensate field in the North Sea (Bendiksen et. al. 1992, Press et al. 1992).

Hasan (Hasan and Kabir 1996) presented a mechanistic model for the flowing temperature of annular gas and the gas/liquid two-phase mixture in the tubing as a function of both well depth and production time, regardless of the well deviation angle. The model was based on energy balance between the formation and fluids flowing through each conduit. While flowing down the annulus, cold gas injected at the wellhead continues to gain heat. The results showed that the temperature profiles in both flow conduits were nonlinear, unlike those used previously, particularly in the annulus.

Kabir, (Kabir et al. 1996) estimated fluid temperature in both flow conduits (drill pipe or tubing, and the annulus) to ascertain the fluid density and viscosity, and in turn to calculate the pressure-drop or the maximum allowable pumping rate for a number of operations. Steady-state heat transfer was assumed in the wellbore while transient heat transfer took place in the formation. A limited sensitivity study showed that all the models gave comparable solutions, with the exception of a line-source solution at early times. In Chapter 3, this model is used to compare the results with the model developed in the study reported here.

George J. Zabaras (Zabaras and Zhang 1997) addressed the thermal performance of the subsea equipment. While subsea insulated flowlines could eliminate or reduce the risk of hydrate formation during steady-state production, they might not provide sufficient cool down time before hydrates were formed during an emergency shutdown. Subsea wellheads, pipe field joints, manifold and flowline tubing jumpers were very

difficult to insulate effectively. As a result, these pieces of equipment exhibited faster cool down to hydrate formation temperature than either the wellbore or the flowline. A two-dimensional general-purpose finite-element partial differential equation solver was utilized to analyze the steady state and transient thermal behavior at different cross-sections of the subsea tree. In contrast to the intuitive common belief that a subsea tree cool down time to hydrate formation temperature was of the order of several hours, a cool down time less than two hours was determined after a system shutdown. Steady-state analysis of a flowline field joint indicated that the joint degrades the flowline thermal performance causing up to a 20% increase in the flowline overall heat transfer coefficient.

Calvert (Calvert and Griffin 1998) described temperatures in wells drilled in deep water. Computer simulations of wellbore temperatures were presented. Additionally, the simulations showed the effects of factors not taken into account by the API correlation (Circ. PS-2018, "Report of Meeting of API Committee 10", 1993, New Orleans, LA). These factors included circulation rate and time, temperature of the injected fluid and sea temperature and currents, to name a few. Failure to account for the correct temperature could result in greatly extended cement setting times and lead to long delays in continued rig operations.

Aadnøy (Aadnøy 1999) developed an analytical model by describing the energy balance in a circulating well. Input of energy due to rotation of the drillstring and pumping of the mud were included. The effect of having a riser in offshore applications was also included. It was shown that for most cases, there was a net flow of energy from the formation to the surface. In offshore applications there would always be a heat loss in the riser. Calculating the energy balance provided important information on temperature- and fluid density behavior. The new analytical model gave improved temperature profiles

throughout the well. In addition to well pressure, this information was also important for cement program design, and in some cases, reservoir PVT analysis. The new models were also different from the older numerical approached as simple model calibration procedures were developed, making the model useful on-site. This paper aimed at implementing these models in field operations.

Chin (Chin et al. 2000) investigated the thermal interaction among the flowlines and its effects on the overall thermal performance of the bundle. Multiphase flow and thermal analysis procedures were conducted for the Garden Banks 216 field pipeline bundle located in the Gulf of Mexico. The investigated bundle had three flowlines that carry multiphase product fluid and heating fluid. The flowlines were enclosed with insulation and encased in a steel casing pipe. The model required a multiphase flow simulator, OLGA, combined with a modified conduction heat transfer model. The numerical analytical results were compared with the field data.

Duret (Duret et al. 2000) developed a transient pipeline bundle numerical module to analyze the thermal interactions between several single phase lines and the main production line. The SYSTUS code developed by SYSTUS International was currently used at Stolt Offshore to solve thermal engineering problems including pipeline bundles. The simulations resulted demonstrate that it was important to take accurately into account thermal effects in case of deep-water production, to predict phenomena such as hydrate formation or wax deposition.

Chen (Chen and Novotny 2003) developed a finite difference method to determine the bottom hole circulating temperature (BHCT) for the proper design of cementing slurries. It also provided the information on temperature recovery after the cement slurry becomes static. Emphasis was placed on evaluation of wells with multiple temperature gradients, multiple fluid circulation schedule, and wellbore deviations. The

effect of offshore water currents was also discussed. The predictions of the wellbore temperature profiles and returned temperatures from this model were validated through actual measured wellbore temperature profile history, including offshore and onshore cases.

Ajay P. Mehta (Mehta, Zabaras et al. 2004) reviewed flow assurance in deep water exploration. Development of a robust flow assurance strategy would play a central role in the system selection, detailed design, and operation of deep water heavy oil fields. Attention was focused on viscosity management techniques and emulsion formation tendencies of heavy oils and also assessed the risk posed by solids such as hydrates, wax and asphaltenes.

Zazovsky (Zazovsky, Haddad et al. 2005) developed a new method for estimating formation temperature from wireline formation tester temperature measurements. This method was based on the reconstruction of thermal history, which involves drilling, no-mud-circulation and pumping-out phases, using the model of heat transport in the formation. The model calibration was achieved by fitting the predicted temperature at some intermediate distance from the borehole for the temperature data measured in flowline during pumping-out. The temperature found in the intermediate zone was then extrapolated to the boundary of the cooled zone surrounding borehole for estimating initial formation temperature. The forward model used for thermal history simulation was simple and robust. It did not involve the borehole temperature modeling during drilling and can be calibrated with a single parameter - either the average mud temperature opposite the tested interval or the average heat flux from the formation during drilling. Although this model could not predict accurately the initial phase of a thermal history (drilling and no-mud-circulation), it became adequate for the pumping out phase when

the details of borehole temperature variation with time during drilling became insignificant.

Ascencio-Cendejas (Ascencio-Cendejas, Reyes et al. 2006) did conceptual studies for the design of thermally bundled wells to optimize the heavy oil production of offshore fields in the Gulf of Mexico. Heat transfer management achieved through novel and clever thermal design, operation and maintenance of the wells, pipelines and process equipment, maintains the viscosity of the oil at acceptable levels.

Piber (Piber, Prohaska et al. 2006) developed a model for cyclic temperature/pressure load tests and the impact of temperature. The ability of Xanthan and Bentonite fluids to break and reestablish viscosity under cyclic temperature and pressure loads was evaluated. Using these findings, the accuracy of hydraulic modeling and nozzle optimization were improved. Better predictions of critical viscosity breakdowns and additive requirements to maintain fluid viscosity were done.

Stiles (Stiles and Trigg 2007) developed a mathematical simulator to model wellbore temperatures. The input parameters for this study were based upon typical deep water well in West Africa. In some of the cases studied, differences among the simulated cementing temperatures were significant enough to warrant performance of risk analysis and implementation of risk mitigation measures. Part two of this paper presented the circulating temperature model and temperature surveillance program utilized to drill and test a deep water high temperature high pressure (HTHP) wells. The predictions from the model were used to evaluate design considerations, such as the selection of blowout preventer (BOP) elastomers and qualification of downhole drilling and testing tools. The model aided in completion fluid selection to optimize hydrate prevention and influence flowing wellhead and surface temperatures. A comparison of modeled parameters and measured field data was included. In addition to the model results, the functionalities of

each of the temperature simulators and how those functionalities might influence the results were discussed.

Tahmourpour (Tahmourpour and Quinton 2009) discussed how best practices in combination with optimized downhole temperature modeling could potentially reduce the number of hours in wait-on-cement-time without introducing any additional risk factors into the cementing/drilling operations. Calculating accurate downhole temperature and pressure profiles, which were also used for pipe-body movement and casing-and tubing-load analysis, assists cementing, drilling, and completion engineers to produce a highly effective solution.

Izgec (Izgec, Hasan et al. 2010) used a wellbore model handling steady flow of fluids but unsteady-state heat transfer to estimate production rate, given wellhead pressure and temperature. The model rigorously accounted various thermal properties of the fluid and the formation, including Joule-Thompson (J-T) (Thompson and Joule 1853) heating and/or cooling. In the single-point approach, a single-point-temperature measurement made anywhere in the wellbore, including at the wellhead, was needed to estimate the mass rate at a given time step. Good correspondence between the measured and calculated resulted demonstrates the robustness of the proposed methods.

Chapter 2: Mathematical and Numerical Model

In this chapter, the mathematical model that drives the heat transfer processes during a drilling operation was presented. Assumptions to simplify the equation systems and decouple energy conservation equation from mass and momentum conservation equations were also discussed in this chapter.

Due to the complexity of the problem, analytical models are not very efficient to obtain the temperature distribution, as they require many simplifications. In this chapter, along with the mathematical model, a numerical solution method to the problem was also presented. Using numerical solution techniques, the differential equations were converted into linear equation systems which can be solved with direct or iterative linear solvers. It is possible to approach this problem using different numerical methods such as finite difference, finite volume, or finite element. Finite volume method is one of the most common numerical methods for the problems involving mass, momentum, and energy transport, as it is based on the conservation principle of the unknown quantity.

The process of circulation consists of 3 stages: (1) fluid enters the drill pipe with a known flow rate and specified temperature and flows down in z direction, (2) fluid exits the drill pipe through the bit and enters the annulus at the bottom, (3) the fluid flows up in the annulus and exits the annulus (Figure 2-1). For reverse circulation the flow direction is down in the annulus and up in the drill pipe. In both cases, there is a cross flow and therefore heat transfer between the fluids in the drill pipe and annulus via convection and also conduction through piping. In addition, the fluid in the annulus the formation exchanges heat as well. Generally, the formation temperature is lower than the annulus fluid temperature at locations closer to the surfaces; however for deeper locations

formation temperature exceeds the annular fluid temperature. Therefore, circulation of mud cools down the near wellbore formation for deeper locations.

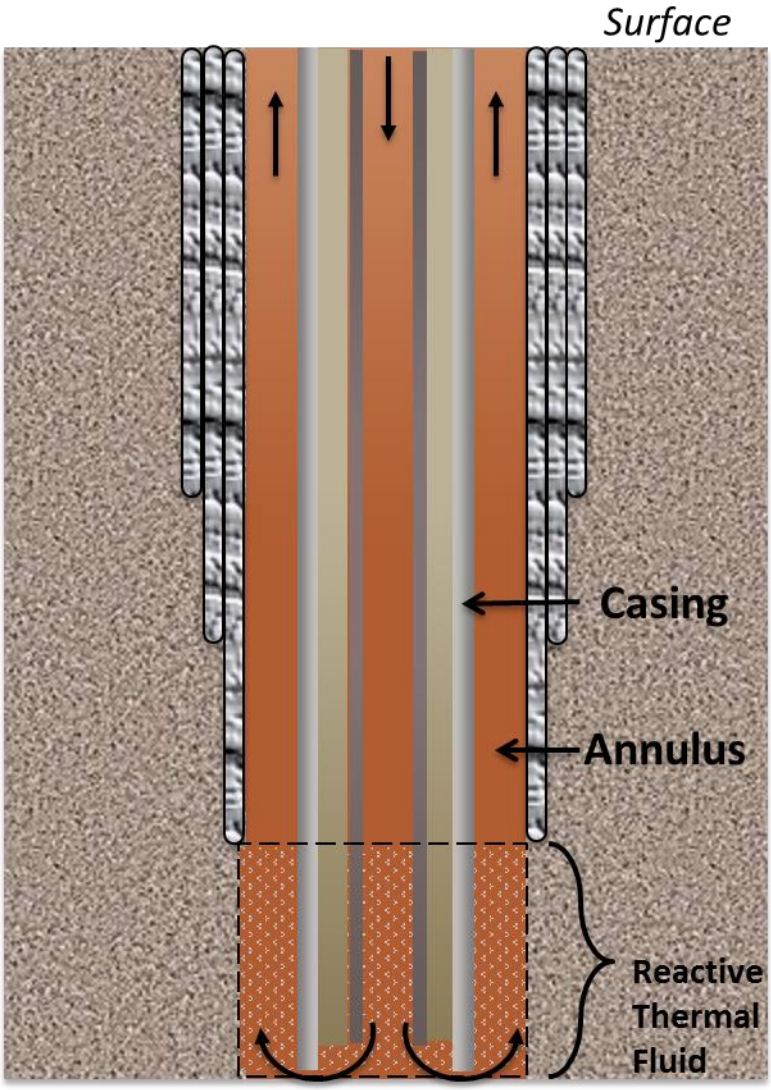

Figure 2-1: Diagram of the heat transfer problem

2.1 GOVERNING EQUATIONS

In the most general approach, in order to be able to investigate the temperature distribution of the wellbore, coupled equations for mass, momentum, and energy

transport should be solved simultaneously, since some of the parameters of the problem depend on the solutions of all three equations. In addition, since there are different media in the domain of the problem of interest, conservation equations need to be solved for each medium separately and the interactions between these media need to be identified with appropriate boundary conditions.

2.1.2 Assumptions and simplifications

In order to simplify the mathematical model, various assumptions can be made. One of the most reasonable yet very simplifying assumption is to decouple energy conservation equation and mass and momentum transport equations. Physically, this assumption states that the temperature distribution does not affect the velocity field and the continuity, or vice versa. This approach also assumes that mass is preserved; therefore the fluid loss to the formation is ignored. Since momentum and energy transport equations are decoupled, the momentum transport equation needs to be solved or a velocity field needs to be assumed prior to the solution of energy equation. For this study uniform velocity was assumed, i.e., velocity is not a function of radial or vertical position. Therefore, the energy equation (Eq. 2.1) was solved without momentum or mass conservation equations.

$$\frac{\partial}{\partial t}(\rho h) + \nabla \cdot (\rho \mathbf{U} h) = \nabla \cdot (\mathrm{k} \nabla T) + S \tag{2.1}$$

In addition, the material properties of the fluid and the formation such as density, specific heat capacity, thermal conductivity, and viscosity were assumed to be independent of temperature. These assumptions help to linearize the problem which makes the solution much faster computationally.

The coordinate system was chosen to be cylindrical and the domain of the problem was assumed to be axisymmetric, i.e., no eccentricity was present. This assumption reduces the problem to 2 dimensions rather than 3 dimensions, eliminating the angular position.

Along with those major assumptions, some additional minor assumptions were also made, such as neglecting thermal expansion, viscous dissipation etc.

2.2 FINITE VOLUME DISCRETIZATION

The finite volume method is one of the most common numerical methods for problems regarding mass, momentum, and heat transport. The discretization technique of the finite volume method expresses the conservation principle for the unknown variable. The most useful feature of this method is that the resulting solution of each grid element and therefore the overall system ensures the conservation principles.

The general transport equation as shown in the mathematical model can be written as follows for any scalar quantity that is being transported:

$$\frac{\partial}{\partial t}(\rho\phi) + \nabla \cdot (\rho \mathbf{U}\phi) = \nabla \cdot (\Gamma \nabla\phi) + S \tag{2.2}$$

The above equation consists of four terms: the transient accumulation term, the convection term which represents the contribution of transport carried by the velocity field, the diffusion term, and the generation term. The variable ϕ can be substituted by 1 for mass transport, by the magnitude of the respective velocity component for momentum transport for three directions, and by enthalpy for energy transport. Therefore, with the appropriate substitutions, the energy conservation equation becomes:

$$\frac{\partial}{\partial t}(\rho h) + \nabla \cdot (\rho \mathbf{U} h) = \nabla \cdot (\mathrm{k} \nabla T) + S \tag{2.3}$$

It is possible to write enthalpy in terms of specific heat capacity and temperature for ideal gases, liquids, and solids.

$$dh = cdT \tag{2.4}$$

Therefore, the energy conservation equation can be written in terms of temperature in the following way:

$$\frac{\partial}{\partial t}(\rho cT) + \nabla \cdot (\rho \mathbf{U} cT) = \nabla \cdot (k \nabla T) + S \tag{2.5}$$

$$\frac{\partial}{\partial t}(\rho cT) + \nabla \cdot \mathbf{J} = S \tag{2.6}$$

$$\mathbf{J} = \rho \mathbf{V} cT - k \nabla T \tag{2.7}$$

In order to discretize the differential equation to get algebraic equations, the energy equation was integrated over the control volume and the time step. In order to be able to perform the integration, certain profile assumptions are required.

$$\int_{\Delta V} \int_{\Delta t} \frac{\partial}{\partial t}(\rho cT) dt\, dV + \int_{\Delta t} \int_{\Delta V} \nabla \cdot \mathbf{J} dV dt = \int_{\Delta t} \int_{\Delta V} S dV dt \tag{2.8}$$

The order of the integration was changed for operational convenience purposes for flux and the source term, as this is a legitimate operation for integral operation.

$$\int_{\Delta V} [(\rho cT)^{t_1} - (\rho cT)^{t_0}]\, dV + \int_{\Delta t} \int_{A} \mathbf{J} \cdot dA dt = \int_{\Delta t} \int_{\Delta V} S dV dt \tag{2.9}$$

The integration of the unsteady term over time can be seen as the difference between the two time steps. The volume integral of the flux term is transferred to an area

integral using the Divergence Theorem. In order to integrate the unsteady term over the volume, a temperature profile was assumed over the control volume. The simplest possibility is to assume that the temperature at the grid point P prevails over the control volume surrounding it. The same assumption can be made for the source term as well. The area integral of the flux term yields the summation of the net effluxes through all of the faces.

$$\int_{\Delta V} \rho cT \, dV = (\rho cT)_P \Delta V \tag{2.10}$$

$$\int_{\Delta V} S dV = \bar{S} \Delta V \tag{2.11}$$

$$\left[(\rho cT)_P^{t_1} - (\rho cT)_P^{t_0}\right]\Delta V + \int_{\Delta t} \sum_{f=e,w,n,s} \mathbf{J}_f \cdot \mathbf{A}_f dt = \int_{\Delta t} \bar{\mathrm{S}} \Delta V dt \tag{2.12}$$

To perform the last step of the discretization, the flux terms and the source term need to be integrated over time. Since those terms may not be the same for two subsequent time steps, it is not obvious which value to use to evaluate them. However, it is possible to assume that the change is linear over the time step and the result of the integral is a combination of the previous and current time step values.

$$\int_{\Delta t} \mathbf{J} \cdot \mathbf{A} dt = (f\mathbf{J}^{t_1} \cdot \mathbf{A} + (1-f)\mathbf{J}^{t_0} \cdot \mathbf{A})\Delta t \tag{2.13}$$

$$\int_{\Delta t} \bar{S} \Delta V dt = (f\bar{S}^{t_1}\Delta V + (1-f)\bar{S}^{t_0}\Delta V)\Delta t \tag{2.14}$$

$$\begin{aligned}\left[(\rho cT)_P^{t_1} - (\rho cT)_P^{t_0}\right]\Delta V + (f\mathbf{J}^{t_1} \cdot \mathbf{A} + (1-f)\mathbf{J}^{t_0} \cdot \mathbf{A})\Delta t \\ = (f\bar{S}^{t_1}\Delta V + (1-f)\bar{S}^{t_0}\Delta V)\Delta t\end{aligned} \tag{2.15}$$

In order to make sense of this equation, different values of the interpolation constant, f, must be assumed. The two most common assumptions are 0 and 1, i.e., the flux values are calculated either at the previous time step or at the current time step. They are called explicit and implicit time schemes, respectively, due to the nature of the algebraic equation set they ultimately result it. The first one gives an equation set where the unknown values can be written in terms of the known values explicitly; for the second approach an equation set is obtained where the unknown parameters can be obtained through a solution method for linear equation systems.

2.2.1 Explicit Scheme

The explicit scheme is a special case of time integration methods where the interpolation factor, f, is taken to be 0, i.e., the flux and the source terms are calculated in the previous time step and assumed to be constant at that value until the next time step. Therefore the discrete equation set takes the following form:

$$\left[(\rho cT)_P^{t_1} - (\rho cT)_P^{t_0}\right]\Delta V + \sum \mathbf{J}^{t_0} \cdot \mathbf{A}\,\Delta t = \bar{S}^{t_0}\Delta V \Delta t \tag{2.16}$$

$$\rho c \frac{T_P^{t_1} - T_P^{t_0}}{\Delta t}\,\Delta V + \sum \mathbf{J}^{t_0} \cdot \mathbf{A} = \bar{S}^{t_0}\Delta V \tag{2.17}$$

The physical meaning of the above equation is that the sum of the accumulation of the energy and the net effluxes is equal to the generated energy. When the steady state is reached, the temperature at any point for two subsequent time steps become the same, making the accumulation term zero. The rest of the equation is the steady-state heat transfer equation. Therefore, the time-dependent solution ultimately reaches to the steady state.

In the explicit time scheme the only unknown is the temperature at point P at the time step $t + 1$. Hence, the equation can immediately be solved for all of the points in the discrete domain and marching in time, without any need for a linear solver.

2.2.2 Implicit Scheme

The implicit scheme is another special case of time integration methods where the interpolation factor, f, is taken to be 1, i.e., the flux and source terms are assumed to be constant at the new time step value. The discrete equation can be written in the following way:

$$\rho c \frac{T_P^{t_1} - T_P^{t_0}}{\Delta t} \Delta V + \sum \mathbf{J}^{t_1} \cdot \mathbf{A} = \bar{S}^{t_1} \Delta V \tag{2.18}$$

The physical meaning of the energy conservation equation and the steady state behavior is the same as explicit scheme. The major difference is that the flux terms, and sometimes the source term depending on its nature, include temperature values of neighboring points which are unknown. Therefore, we have one equation with more than one unknown parameters which cannot be solved on its own. To be able to solve this system, the above equation needs to be written for all of the points. For a discrete domain with N nodes, this would result in N equations with N unknowns which are nodal temperatures. Then, this equation set can be solved using linear algebra techniques. Although implicit time scheme requires more computational effort for a time step, it can be more advantageous due to the fact that it allows for large time steps without any stability problems whereas explicit time scheme has a certain time step limit due to stability concerns.

2.2.3 Flux Terms

The flux terms may include both conduction and convection terms. Both conduction and convection terms require some assumptions, since the fluxes are calculated at the cell faces, whereas the temperatures are calculated at the cell centroids.

For example, the conduction term at the east face of the cell around point P can be expressed in the following way:

$$\mathbf{J_e} \cdot \mathbf{A_e} = -kA_e \left(\frac{\partial T}{\partial x}\right)_e \tag{2.19}$$

This requires the calculation of the x derivative of the temperature at the cell face. With the assumption of linear profile between the nodes P and E, the flux term can be written in terms of temperatures in the following way:

$$\mathbf{J_e} \cdot \mathbf{A_e} = -kA_e \frac{T_E - T_P}{\delta x_e} = kA_e \frac{T_P - T_E}{\delta x_e} \tag{2.20}$$

The convective flux term can be expressed as follows:

$$\mathbf{J_n} \cdot \mathbf{A_n} = (\rho cuT)_n A_n \tag{2.21}$$

Since we are calculating the flux term at the boundary, we need the temperature value at the boundary. However, the temperature values are stored in the cell centroids. Therefore, another profile assumption is required. Similar to conductive flux, a linear profile assumption can be made and the average of the two neighboring nodes can be taken as the face value. This approach is called Central Difference Scheme (CDS) and may result in some stability problems. Another approach is so called Upwind Difference Scheme (UDS) which suggests taking the value of the node at the upwind direction. This is a valid assumption for most of the convection-dominant heat transfer problems (Minkowycz et al. 2006. Handbook of Numerical Heat Transfer).

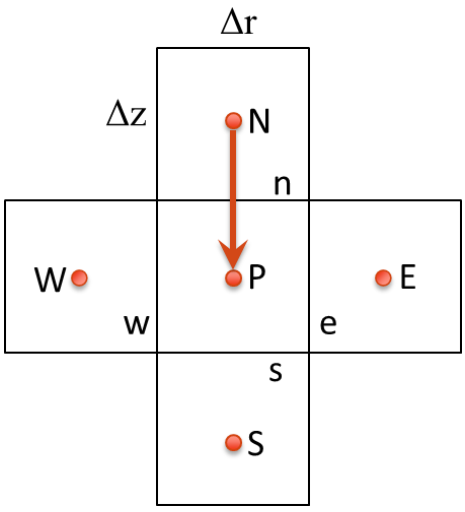

Figure 2-2: Cells around an arbitrary point P and its neighbor points

For the domain shown in the Figure 2-2, and the flow in the shown direction the energy conservation equation can be written discretely in the following form for the explicit scheme:

$$\rho c \frac{(T_P^{t+1} - T_P^t)}{\Delta t} \Delta V + (\rho c u_z A_n)_n T_N^t - (\rho c u_z A_s)_s T_P^t + k_e \frac{(T_P^t - T_E^t)}{\Delta r} A_e + k_w \frac{(T_P^t - T_W^t)}{\Delta r} A_w + k_n \frac{(T_P^t - T_N^t)}{\Delta z} A_n + k_s \frac{(T_P^t - T_S^t)}{\Delta z} A_s = S\Delta V \tag{2.22}$$

$$a_P T_P = a_P^0 T_P^0 + \sum a_{nb} T_{nb}^0 + b \tag{2.23}$$

$$a_e = \frac{k_e A_e}{\Delta r} \tag{2.24}$$

$$a_w = \frac{k_w A_w}{\Delta r} \tag{2.25}$$

$$a_n = \frac{k_n A_n}{\Delta z} \tag{2.26}$$

$$a_s = \frac{k_s A_s}{\Delta z} + (\rho c u_z A_s)_s \tag{2.27}$$

$$a_P = \frac{\rho c \Delta V}{\Delta t} \tag{2.28}$$

$$a_P^0 = a_P - a_e - a_w - a_n - a_s + (\rho c u_z A_s)_s - (\rho c u_z A_n)_n \tag{2.29}$$

$$b = S\Delta V \tag{2.30}$$

As aforementioned, the explicit scheme has stability problems. For numerical schemes in the above form, the coefficients must be nonnegative. Otherwise, the numerical solution would result in nonphysical solutions. A negative coefficient of a temperature value, whether it is a neighbor node temperature or previous time step value of the point P, implies that increasing temperature at a point decreases the temperature in its vicinity, which is not physical. Therefore, problems with negative coefficients tend to give erroneous solutions which most of the times, the solution diverge and go to infinity.

The coefficient, a_p^0, has both positive and negative terms. Depending on their relative magnitude the term may become negative and thus unstable. This restricts the magnitude of the time step, depending on the material properties and the element size.

For the same domain and flow conditions, the flux terms can be written for the implicit scheme in the following form:

$$\rho c\frac{(T_P^{t+1}-T_P^t)}{\Delta t}\Delta V+(\rho cu_zA_n)_nT_N^{t+1}-(\rho cu_zA_s)_sT_P^{t+1}$$
$$+k_e\frac{(T_P^{t+1}-T_E^{t+1})}{\Delta r}A_e+k_w\frac{(T_P^{t+1}-T_W^{t+1})}{\Delta r}A_w \tag{2.31}$$
$$+k_n\frac{(T_P^{t+1}-T_N^{t+1})}{\Delta z}A_n+k_s\frac{(T_P^{t+1}-T_S^{t+1})}{\Delta z}A_s=S\Delta V$$

$$a_PT_P=a_P^0T_P^0+\sum a_{nb}\,T_{nb}+b \tag{2.32}$$

$$a_e=\frac{k_eA_e}{\Delta r} \tag{2.33}$$

$$a_w=\frac{k_wA_w}{\Delta r} \tag{2.34}$$

$$a_n=\frac{k_nA_n}{\Delta z} \tag{2.35}$$

$$a_s=\frac{k_sA_s}{\Delta z}+(\rho cu_z\Delta r)_s \tag{2.36}$$

$$a_P^0=\frac{\rho c\Delta V}{\Delta t} \tag{2.37}$$

$$a_P=a_P^0+a_e+a_w+a_n+a_s-(\rho cu_z\Delta r)_s+(\rho cu_z\Delta r)_n \tag{2.38}$$

$$b=S\Delta V \tag{2.39}$$

Unlike the explicit scheme, there is no possibility for negative coefficients, as long as the continuity is satisfied. Therefore, larger time steps can be chosen in order to decrease the computational time.

The equation above consists of 5 unknown values, namely the temperatures at the point P and at its four neighbors. Therefore, the same equation must be written in all N

nodes in the system, resulting in an NxN linear system. Then, either a direct or iterative linear solver can be used to solve the system of equations.

2.3 Boundary Conditions

The application of the energy conservation is slightly different for boundary nodes compared to inner nodes. Due to the symmetric nature of the problem, one half of the domain is modeled. In that case, the inner boundary condition will be an adiabatic boundary condition, a special case of Neumann (Minkowycz et al. 2006. Handbook of Numerical Heat Transfer), where the assigned heat flux to a specific surface is essentially zero (Figure 2-3).

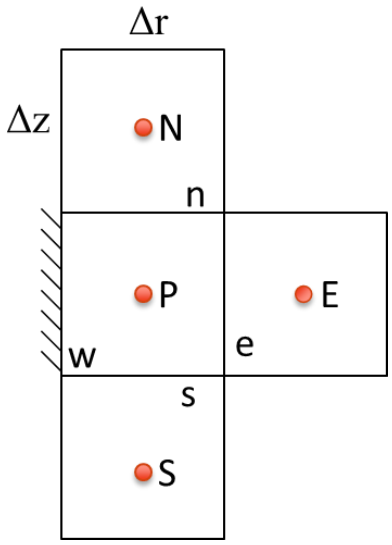

Figure 2-3: The cell with the adiabatic boundary condition

In this case, the energy conversation equation was written by writing the flux through the boundary face –not in terms of the neighboring node, as there is no such node– but using the known flux, which is zero for this case.

The adiabatic boundary condition was assumed for the top and bottom boundaries for the solid domains. A similar discretization was carried out for those boundaries as well.

For the outer boundary condition where the temperature is fixed –Dirichlet boundary condition– the energy conservation equation was written in a similar way as for the inner nodes. The only difference is that the flux from the boundary face was written in terms of a known temperature.

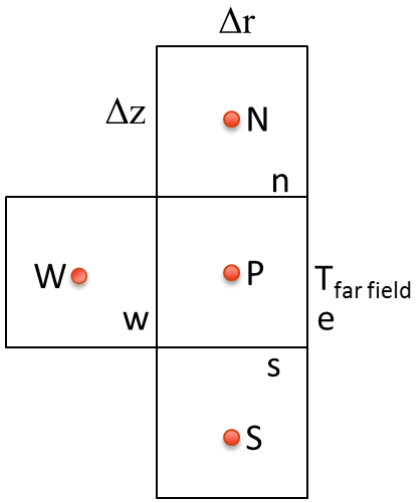

Figure 2-4: The cell with fixed temperature boundary condition

After implementing these boundary conditions, a penta-diagonal matrix was obtained which can be solved using direct or iterative linear solvers. Direct solvers may require long times depending on the number of points in the domain. For finer meshes, i.e., larger coefficient matrices, iterative methods give faster results.

The Gauss Seidel method is one of the most common iterative methods (Minkowycz et al. 2006. Handbook of Numerical Heat Transfer), and it may be a good option for this kind of problems. Line Gauss Seidel is a combination of direct and linear

solvers with a notion similar to Gauss Seidel. A detailed explanation of Line Gauss Seidel can be found in Appendix A.

2.4 IMPLEMENTING THE EFFECTS OF CONVECTION

The numerical analysis developed until this point includes convective heat transfer via mass transport. The cells inside the fluid domain have influxes or effluxes associated with the enthalpy of the incoming or outgoing fluid. Since the flow was assumed to be only in the axial direction in this study, the heat transfer due to mass transport is only in the axial direction. However, this subsequently affects the neighboring nodes in the horizontal direction as well since there is heat interaction in the horizontal direction due to conduction in the fluid. This approach is conceptually correct, since the convective heat transfer is basically conduction and advection. However, when the flow conditions are stronger to ensure better mixing with enhanced heat transfer, this methodology may lead erroneous results. There are possible modifications to improve the accuracy. When the fluid flow is turbulent or near turbulent, the heat transfer in the horizontal direction with the solid surface is enhanced and not bound only to thermal conductivity of the fluid. An effective thermal conductivity can be defined based on analytical and empirical correlations to represent convective heat transfer. Another possible way is to incorporate convective heat transfer correlations for estimation of heat transfer coefficient based on which thermal fluxes between different media can be written. The temperature of the annular and tubular fluids can be modeled as functions of vertical distance using the mean temperature of the fluid in the horizontal direction. Therefore, the heat transfer between annular and tubular fluids as well as annular fluid and the formation in the horizontal direction can be modeled by defining heat transfer coefficients using convection correlations. One drawback of this analysis is the loss of

horizontal temperature distribution information for fluid domains. However, the importance of the horizontal temperature distribution for fluid domains is relatively small.

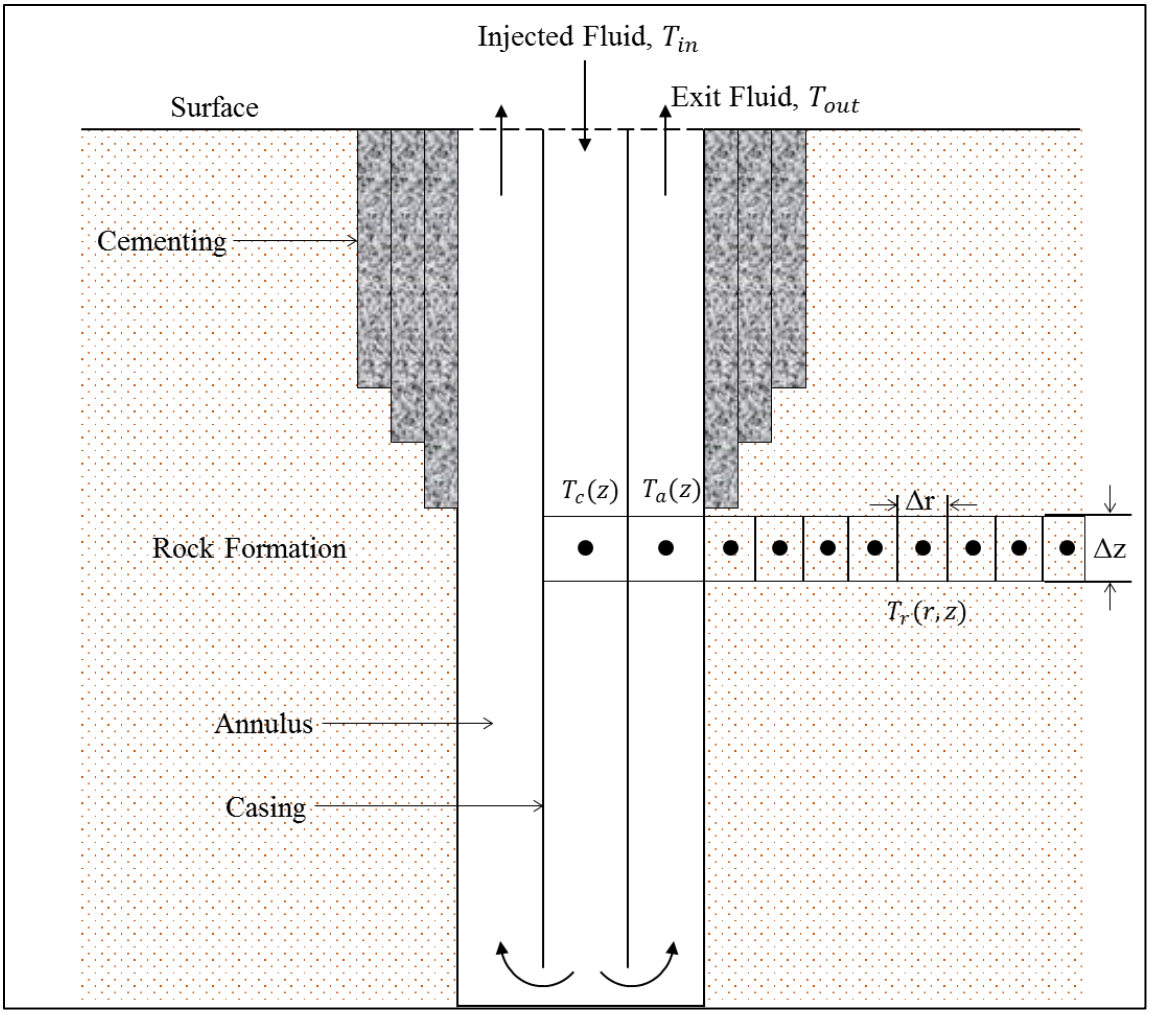

Figure 2-5: Diagram of the numerical model

Figure 2-5 shows the diagram of the numerical model with fluid temperatures being functions of vertical distance. It features a coarse mesh for fluid domains, such that there is only one element in each of them.

Along with the fluid domains, the casing was also excluded. Therefore, an overall heat transfer coefficient between the tubular and annular fluids still needs to be defined. The overall heat transfer coefficient consists of the thermal resistances due to heat transfer coefficients from the fluids to the casing wall, and conductive resistance due to the casing itself as shown in Figure 2-6. The overall heat transfer coefficient between annular and tubular fluids can be written in the following form:

$$\frac{1}{U^{ac}} = \frac{1}{h^c} + \frac{t_c}{k_c} + \frac{1}{h^a} \tag{2.40}$$

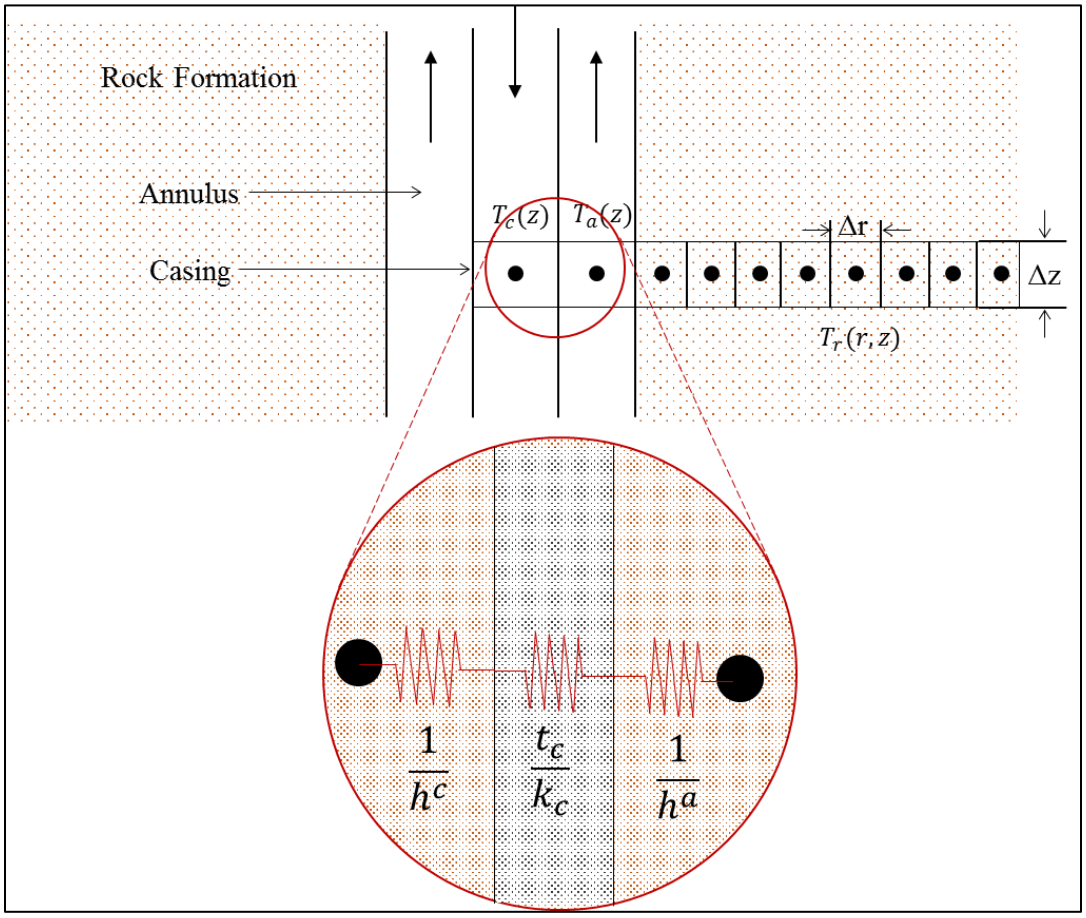

Figure 2-6: Thermal resistances between tubular and annular fluids

The energy balances for tubular and annular fluids can be rewritten in the following forms, for the control volumes shown in Figure 2-6:

$$\rho_l c_l \frac{{T_{c_P}}^{t+1} - {T_{c_P}}^{t}}{\Delta t}\Delta V + (\rho_l u A)_s c_l T_{c_P} - (\rho_l u A)_n c_l T_{c_N} + h^{ac} A^{ac}\left(T_{c_P} - T_{a_P}\right) = S\Delta V \tag{2.41}$$

In a compact form;

$$a_{c_P}^{t+1}\,{T_{c_P}}^{t+1} = a_{c_N} T_{c_N}^{t+1} + a_a T_{a_P}^{t+1} + a_{c_P}^{t}{T_{c_P}}^{t} + b \tag{2.42}$$

$$a_{c_N} = (\rho_l u A)_N c_l \tag{2.43}$$

$$a_a = h^{ac} A^{ac} \tag{2.44}$$

$$a_{c_P}^{t} = \frac{\rho_l c_l \Delta V}{\Delta t} \tag{2.45}$$

$$a_{c_P}^{t+1} = a_{c_N} + a_a + a_{c_P}^{t} - (\rho_l u A)_N c_l + (\rho_l u A)_S c_l \tag{2.46}$$

$$b = S\Delta V \tag{2.47}$$

Similarly for annulus;

$$\rho_l c_l \frac{{T_{a_P}}^{t+1} - {T_{a_P}}^{t}}{\Delta t}\Delta V + (\rho_l u A)_n c_l T_{a_p} - (\rho_l u A)_a c_l T_{a_S} + h^{ac} A^{ac}\left(T_{a_P} - T_{c_P}\right) + h^{w} A^{w}(T_{a_P} - T^{w}) = S\Delta V \tag{2.48}$$

$$a_{a_P}^{t+1}\,{T_{a_P}}^{t+1} = a_{a_s} T_{a_S}^{t+1} + a_c T_{c_P}^{t+1} + a_w T_w + a_{a_P}^{t}{T_{a_P}}^{t} + b \tag{2.49}$$

$$a_{a_S} = (\rho_l u A)_s c_l \tag{2.50}$$

$$a_c = h^{ac} A^{ac} \tag{2.51}$$

$$a_w = h^w A^w \tag{2.52}$$

$$a_{a_P}^t = \frac{\rho_l c_l \Delta V}{\Delta t} \tag{2.53}$$

$$a_{a_P}^{t+1} = a_{a_S} + a_c + a_w + a_{a_P}^t - (\rho_l u A)_S c_l + (\rho_l u A)_N c_l \tag{2.54}$$

$$b = S\Delta V \tag{2.55}$$

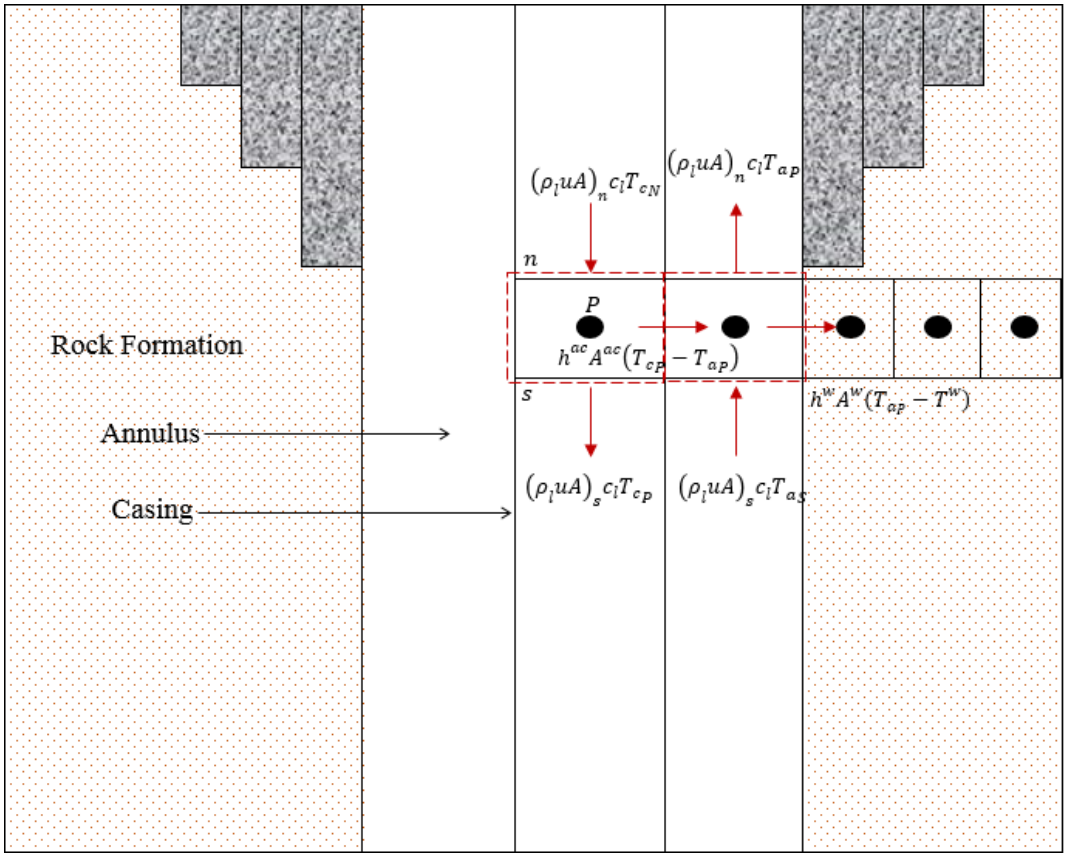

Figure 2-7: Energy balances for fluid domains

Chapter 3: Model Verification

In this chapter, the results of the developed mode were compared to the results obtained with other different approaches to validate the reliability of the model. Although different methods use different simplifications and assumptions, and some of the methods do not cover all of the features of the developed method, the comparison was still possible for some simple cases.

The analytical solution developed by Hasan and Kabir in 1996 (Kabir et al. 1996) as well as commercial software, Drill Bench, were used to compare results obtained from the MATLAB simulation. Both of those methods were primarily used to calculate the fluid temperature and not the formation temperature. Therefore, the comparison was done with the fluid temperatures both for steady state and for different times as the solution goes towards steady state.

3.1 HASAN AND KABIR METHOD

Hasan and Kabir developed an analytical model for wellbore fluid temperature calculation in their work named *A Mechanistic Model for Computing Fluid Temperature Profiles in Gas-Lift Wells (1996)* and *Determining Circulating Fluid Temperature in Drilling, Workover, and Well-Control Operations (1996)* . Their work is one of the many analytical approaches in temperature distribution calculation as discussed in literature review section. In this study, this method was selected for comparison reasons, due to the ease of applicability of the method. It is also very similar to the new computational model developed in this study.

The model was developed to solve a coupled heat transfer problem between tubing, annulus and formation. The heat transfer between different media was represented using heat transfer coefficient correlations. Due to the faster thermal response of the

wellbore as compared to the formation, the temperature profile was assumed to be at steady state within the well bore and unsteady in the formation. The heat transfer from the formation to the well bore was represented via time functions, which are discussed in Ramey's work *Wellbore Heat Transmission (1962)*.

3.1.2 Mathematical Model by Hasan and Kabir

The analysis depends on the fluid circulation direction; however, it is very similar for the two cases. The analysis starts with an energy balance over a differential element dz of annular and tubular fluid. Figure 3-1 shows the energy balance for annular fluid for circulation going down in the annulus and back up in the tubing. q_a is the heat transfer within the annulus due to the fluid flow, q_F is the heat transfer from/to the formation depending on the temperatures of formation and the annulus, and finally q_{ta} is the heat exchange between the annular and tubular fluids.

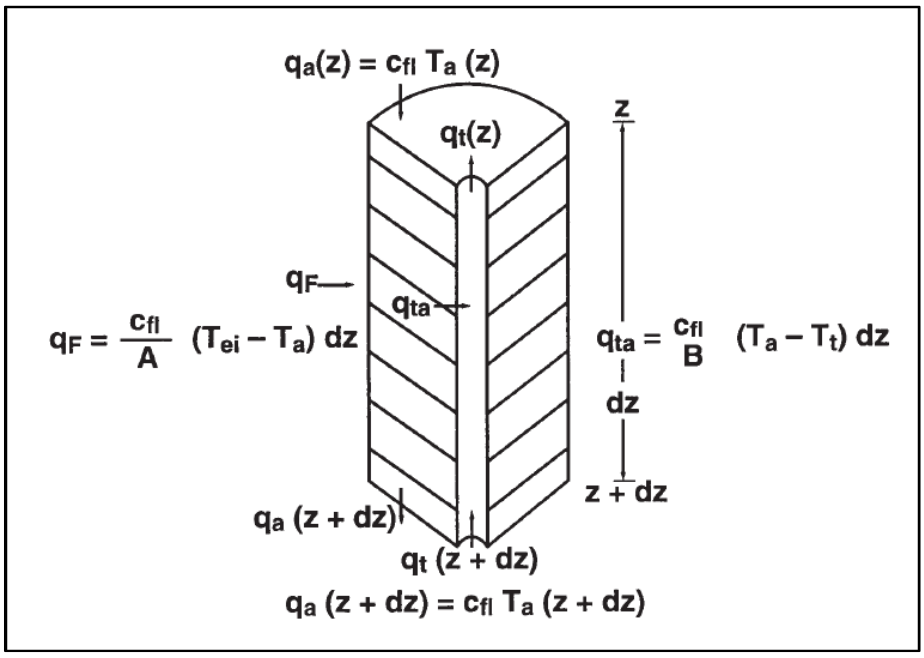

Figure 3-1: Schematic of energy balance for tubing and formation

The energy balance can be written in the following form:

$$q_a(z) - q_a(z + dz) = q_{ta} - q_F \tag{3.1}$$

The energy difference between the inlet and outlet of the control volume can be written in terms of the temperature difference using the specific heat capacity.

$$c_{fl}[T_a(z) - T_a(z + dz)] = q_{ta} - q_F \tag{3.2}$$

The heat transfer in the formation q_F, is estimated using time functions and depends on the inner boundary condition in the following way:

$$q_F = \frac{2\pi k_e}{wT_D}(T_{ei} - T_{wb})dz \tag{3.3}$$

T_D is called dimensionless temperature and can be obtained using different models according to the inner boundary condition.

To eliminate the wellbore temperature, T_{wb}, another relation was written between wellbore temperature and the annular temperature using overall heat transfer coefficient from the annular fluid to the formation.

$$q = \frac{2\pi r_c U_a}{w}(T_{wb} - T_a)dz \tag{3.4}$$

With the steady state assumption, heat transfer from the formation to the annulus q_F equals to q. Therefore, T_{wb} can be eliminated using two equations to give:

$$q_F = \frac{c_{fl}}{A}(T_{ei} - T_a)dz \tag{3.5}$$

$$A = \frac{c_{fl}w}{2\pi}\left[\frac{k_e + r_c U_a T_D}{r_c U_a k_e}\right] \tag{3.6}$$

Heat transfer between the annular and tubular fluids can be written in the following form:

$$q_{ta} = \frac{c_{fl}}{B}(T_a - T_t)dz \tag{3.7}$$

$$B = \frac{wc_{fl}}{2\pi r_t U_t} \tag{3.8}$$

Hence, the energy balance for annular fluid can be rewritten as:

$$c_{fl}[T_a(z) - T_a(z+dz)] = \frac{c_{fl}}{B}(T_a - T_t)dz + \frac{c_{fl}}{A}(T_a - T_{ei})dz \tag{3.9}$$

Rearranging,

$$A\frac{dT_a}{dz} = (T_{ei} - T_a) - \frac{A}{B}(T_a - T_t) \tag{3.10}$$

The final form of the equation has two unknowns: annular and tubular fluid temperatures. A similar energy balance was written for the tubular fluid to obtain the second equation to solve for two unknowns.

$$q_t(z+dz) - q_t(z) = -q_{ta} \tag{3.11}$$

$$c_{fl}[T_t(z+dz) - T_t(z)] = c_{fl}\,\frac{T_t - T_a}{B}dz \tag{3.12}$$

$$\frac{dT_t}{dz} = \frac{T_t - T_a}{B} \tag{3.13}$$

Two equations were obtained to solve for two unknowns. Either T_a or T_t can be eliminated to solve for the other.

$$A\frac{dT_t}{dz} - AB\frac{d^2T_t}{dz^2} = T_{ei} + B\frac{dT_t}{dz} - T_t + A\frac{dT_t}{dz} \tag{3.14}$$

The geothermal gradient, T_{ei} is usually represented as a linear function of the vertical depth as $T_{ei} = T_{es} + g_G z$.

$$AB\frac{d^2T_t}{dz^2} + B\frac{dT_t}{dz} - T_t + T_{es} + g_G z = 0 \tag{3.15}$$

The final form of the equation is a linear second-order ordinary differential equation subject to two boundary conditions: (1) the injection temperature is given, $T_a = T_{as}$ when $z = 0$, (2) the heat transfer between the annular and tubular fluids is zero at the bottomhole, $dT_t/dz = 0$ when $z = H$.

The solutions for annular and tubular temperatures were obtained in the following form:

$$T_t = \alpha e^{\lambda_1 z} + \beta e^{\lambda_2 z} + g_G z + B g_G + T_{es} \tag{3.16}$$

$$T_a = (1 - \lambda_1 B)\alpha e^{\lambda_1 z} + (1 - \lambda_2 B)\beta e^{\lambda_2 z} + g_G z + T_{es} \tag{3.17}$$

For the conventional circulation direction, for which the fluid goes down in the casing and flows back up through the annulus, the analysis is very similar and the temperatures are given in the following form:

$$T_t = \gamma e^{\xi_1 z} + \delta e^{\xi_2 z} + g_G z - B g_G + T_{es} \tag{3.18}$$

$$T_a = (1 + \xi_1 B)\gamma e^{\xi_1 z} + (1 + \xi_2 B)\delta e^{\xi_2 z} + g_G z + T_{es} \tag{3.19}$$

The constants $\alpha, \beta, \lambda_1, \lambda_2, \gamma, \delta, \xi_1, \xi_2$ are given in Appendix B.

3.2 Comparison with Hasan and Kabir and Drill Bench Results

The analysis of Hasan and Kabir assumes steady state behavior in the wellbore. A similar analysis was done by Ramey as well. The accuracy of results was higher for longer periods of circulation (Ramey 1962). Therefore, the analysis of Hasan and Kabir were used to compare the steady state behavior of the fluid temperature and the results were compared to the results obtained from the MATLAB simulation and also using Drill Bench for long circulation times. The MATLAB model and Drill bench simulation were

run for 1000 minutes of real time circulation and the results were compared to Hasan and Kabir's steady state solution.

A crucial point for the calculations is the estimation of heat transfer coefficient between different media. Although Hasan and Kabir use some convection correlation between different media, the value of the heat transfer coefficients or the correlation to obtain that value were not specified or cited. Along with the heat transfer coefficients, other parameters such as tubing wall thickness, tubing material thermal conductivity also affect overall heat transfer coefficients.

Similarly for Drill Bench, although some dimensionless parameters such as Reynolds number can be obtained as output, heat transfer coefficient or the required parameters such as Nusselt number, Prandtl number, heat transfer correlations to calculate heat transfer coefficient cannot be obtained. Therefore, to be able to compare different methods, these parameters must be adjusted accordingly.

The parameters used in the calculations are shown in Table 3-1.

Table 3-1: Problem Parameters for Comparison with Hasan and Kabir and Drill Bench

Geometry				
Casing OD	0.1397	m	5 ½	in
Casing ID	0.1651	m	6 ½	in
Annulus Clearance	0.0254	m	1	in
Far field distance	0.5	m	1.64	ft
Depth	4200	m	14000	ft

Material Properties			
	Density (kg/m^3)	Specific Heat Capacity (kJ/kgK)	Thermal Conductivity (W/mK)
Fluid	1384	2500	1.02
Casing	7840	800	50
Formation	2500	1200	2.2

Other Parameters				
Circulation Rate	10	kg/s	115	gal/min
Injection Temperature	26.67	°C	80	°F
Surface Temperature	26.67	°C	80	°F
Temperature Gradient	0.01823	°C	0.01	°F/ft

A Drill Bench model was created with the parameters given in Table 3-1. The parameters that cannot be entered into Drill Bench as input or taken as output, namely

heat transfer coefficients, were then adjusted for the Hasan and Kabir solution such that the steady state solution of Drill Bench matches Hasan and Kabir solution.

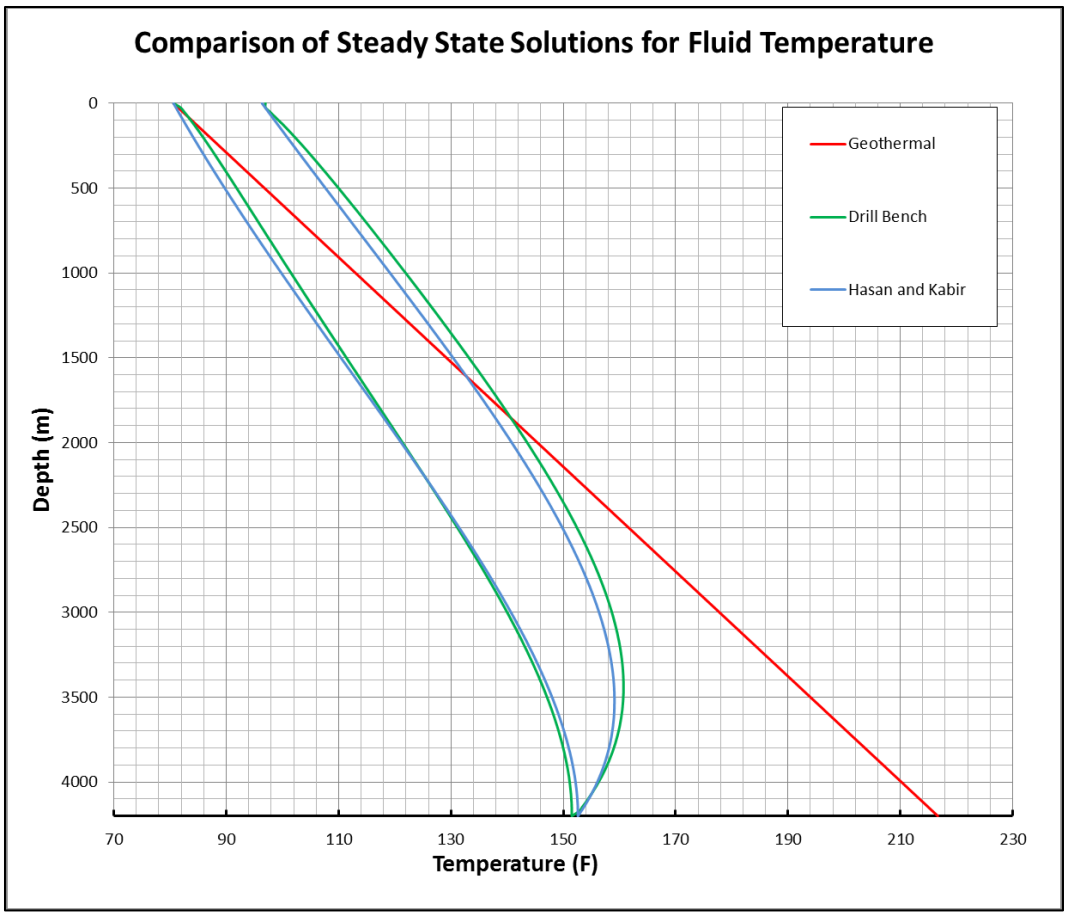

Figure 3-2: Comparison of Hasan and Kabir and Drill Bench Steady State Temperatures

Figure 3-2 shows the results obtained from Drill Bench and Hasan and Kabir, for tubular and annular fluid temperatures as well as the geothermal gradient. The overall heat transfer coefficient used in Hasan and Kabir was adjusted, such that the two results have a reasonably good match. The heat transfer coefficients between the tubular and annular fluid and annular fluid and the formation were taken to be 50 W/mK.

When the heat transfer coefficient values were set to the same value for the MATLAB simulation, the final temperature distribution was somewhat different. This is understandable because different approaches result in different temperature distributions due to inherent different assumptions. But it is important that the trend is essentially the same.

A similar heat transfer coefficient adjustment can be done for the MATLAB simulation as well to get a better match between the results of different approaches. Another thing to note is that the heat transfer coefficients assumed for Hasan and Kabir's analysis are not based on the convection correlations or the input parameters of the Drill Bench simulation. Therefore, it is reasonable to make a similar calibration for the MATLAB simulation as well. Figure 3-2 shows the comparison of all three methods with the same heat transfer coefficient. The bottomhole temperature calculated by MATLAB simulation is about 10 °F colder than the other two methods. Although the trends of all three temperature distributions obtained from different methods are similar, there is a considerable difference quantitatively. The largest difference between the temperatures is within the section between 3000 – 3500 m from the surface and it is around 20 °F.

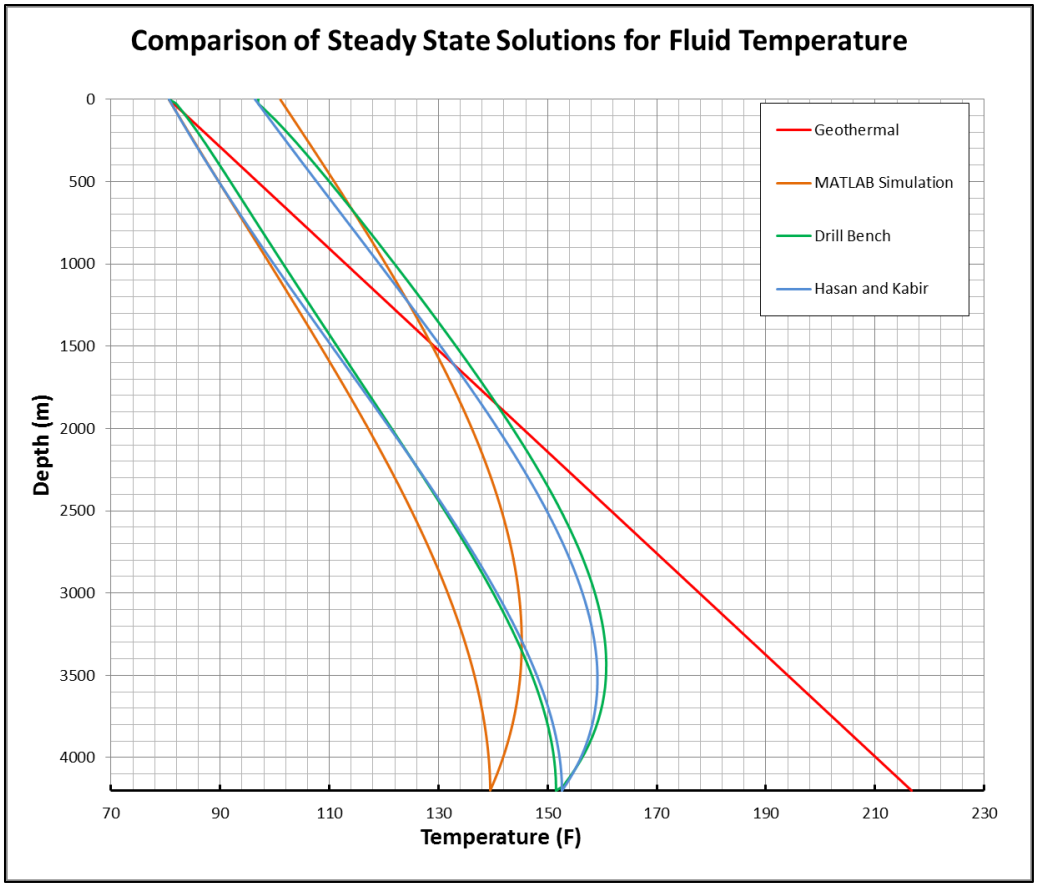

Figure 3-3: Comparison of steady state temperature distribution of 3 methods

The heat transfer coefficient between annular and tubular fluids as well as between annular fluid and the formation were adjusted to match the Drill Bench results. The bottomhole temperature increases as the heat transfer coefficients increase, since the energy interaction between the fluids and the hotter formation is enhanced when the heat transfer coefficient increases. Since with this heat transfer coefficient, the bottomhole temperature calculated by MATLAB simulation is lower than the other two methods, a higher heat transfer coefficient needs to be chosen. Figure 3-3 shows the comparison of all three methods with adjusted heat transfer coefficients. The agreement of the results is very good for most purposes. The bottomhole temperatures agree within a margin of 1.5

°F. The bottomhole temperatures calculated by MATLAB, Drill Bench and the Hasan and Kabir methods are 149.8 °F, 151.3 °F, and 152.6 °F, respectively. The largest difference between the results are again at a depth of around 3500 m from the surface. The difference is about 7 F with temperatures calculated at 3500 m being 153.2 F, 160.1 F, and 159.1 F for MATLAB simulation, Drill Bench and the Hasan and Kabir analysis, respectively.

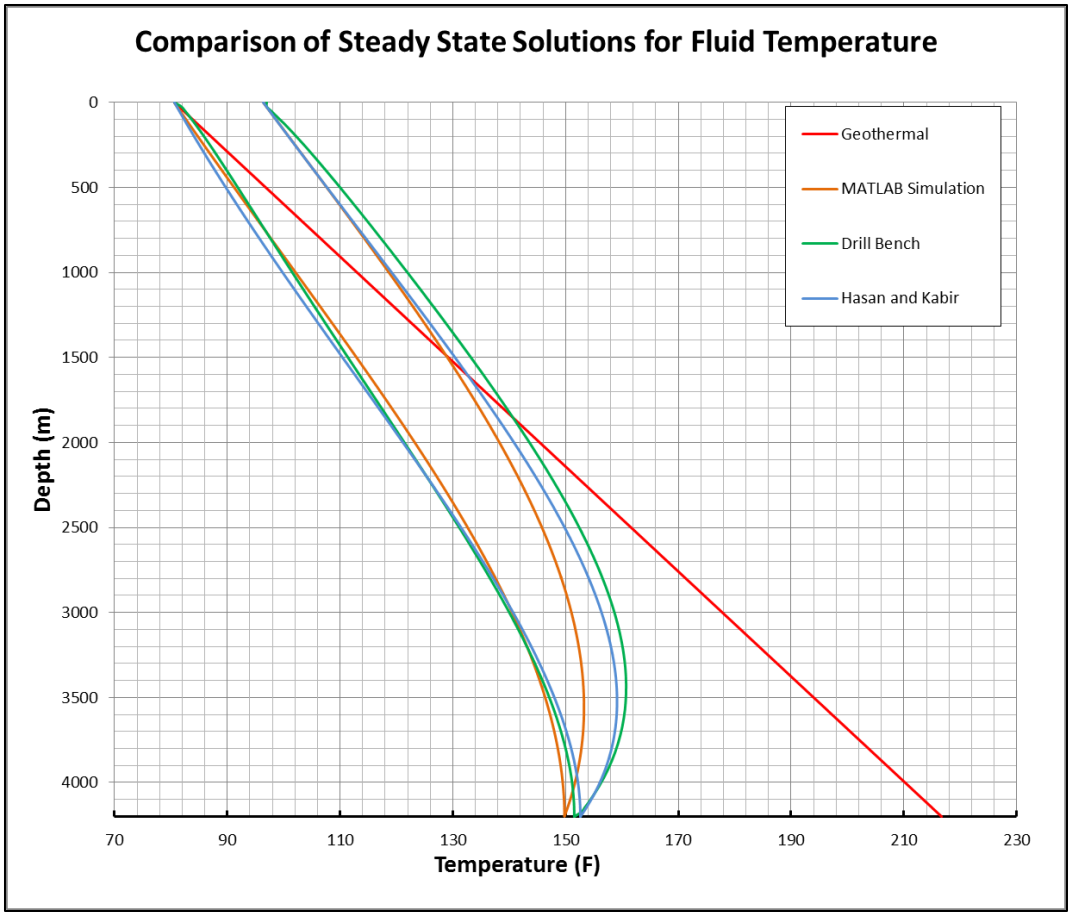

Figure 3-4: Comparison of steady state behavior of 3 methods with adjusted heat transfer coefficients

Along with the steady state behavior, it is also important to compare transient behavior of the thermal response. For that comparison, the Hasan and Kabir analytical method is of no use, as the solution method calculates the wellbore temperatures based on the assumption that the heat transfer in the wellbore is steady state. However, Drill Bench and MATLAB simulation can still be compared for transient response of the temperature for the annular and tubular fluids.

Figure 3-5 shows the bottomhole temperature as a function of time. The expected trend of the time response of the bottom hole temperature is exponential. Both MATLAB and Drill Bench results follow an exponential behavior. The difference between the two methods is about 10 °F at around 150 minutes. The behavior of the Drill Bench result clearly changes at about 100 minutes. This may be due to some change in the problem parameters. MATLAB model assumes that the simulation parameters are constant throughout the analysis. Material properties and other simulation parameters like heat transfer coefficient were not defined as functions of temperature or pressure. The most likely reason for the behavior change in Drill Bench would be a change in the material properties or heat transfer coefficient at 100 minutes.

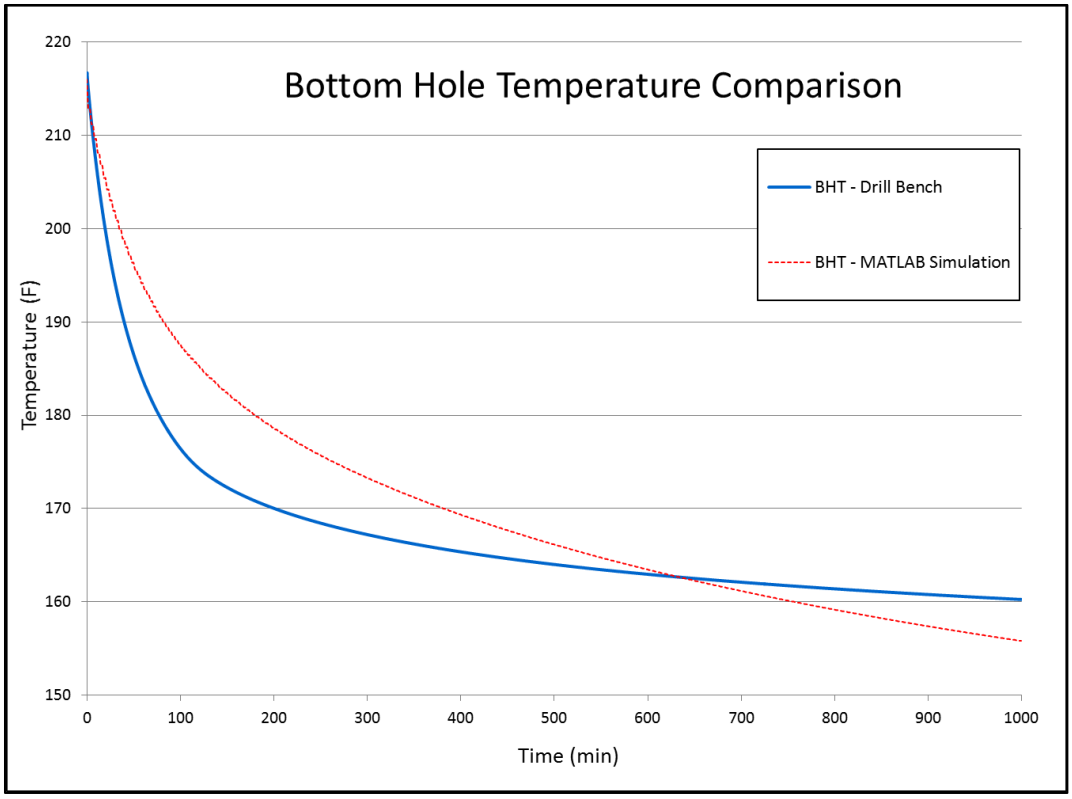

Figure 3-5: Transient behavior of Bottom Hole Temperature

Apart from the bottom hole temperature, it is also important to compare the temperature distribution along the wellbore at different times. Although there is a quantitative difference between the results obtained from the two approaches, the results match each other quite well qualitatively.

Figure 3-6, 3-7, and 3-8 shows the temperature distributions along the well for 1, 2, and 10 hours, respectively, after circulation starts.

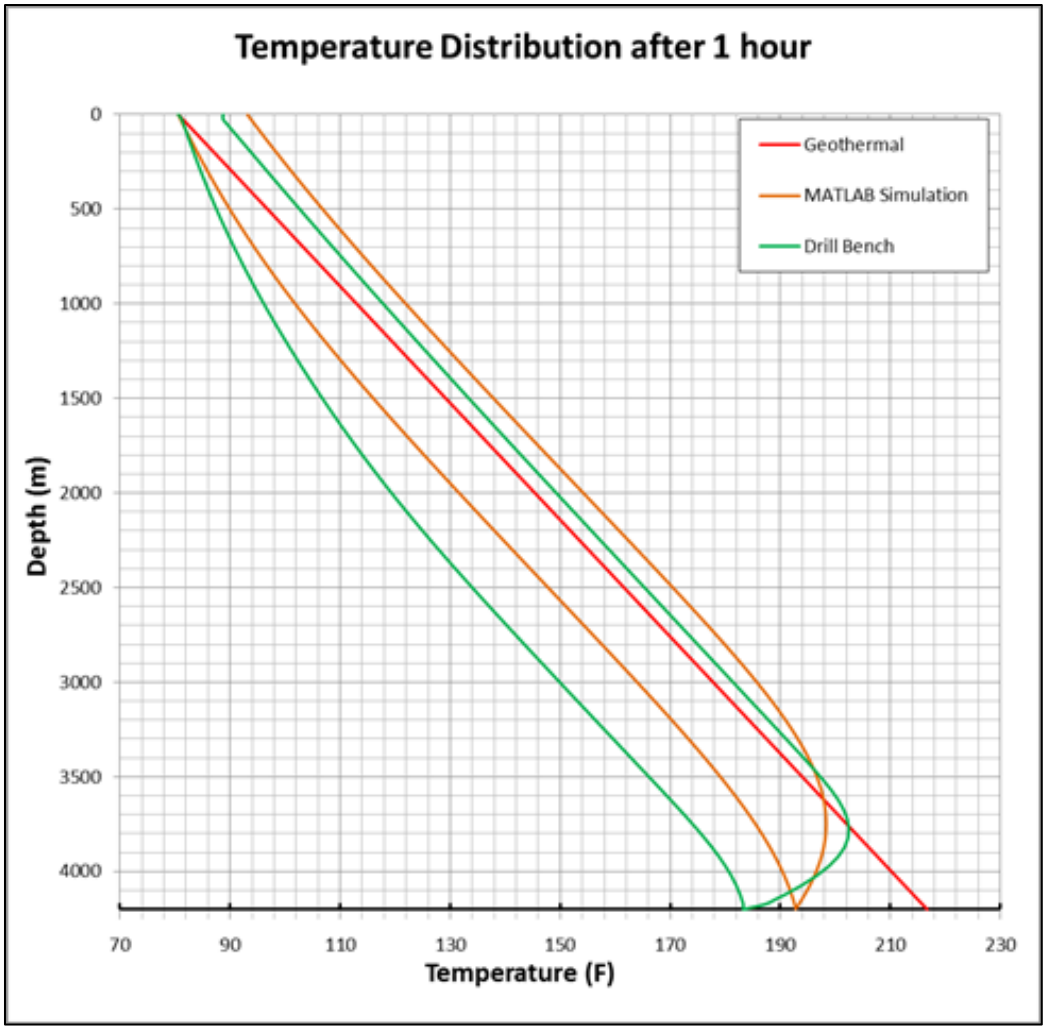

Figure 3-6: Comparison of temperature distribution after 1 hour

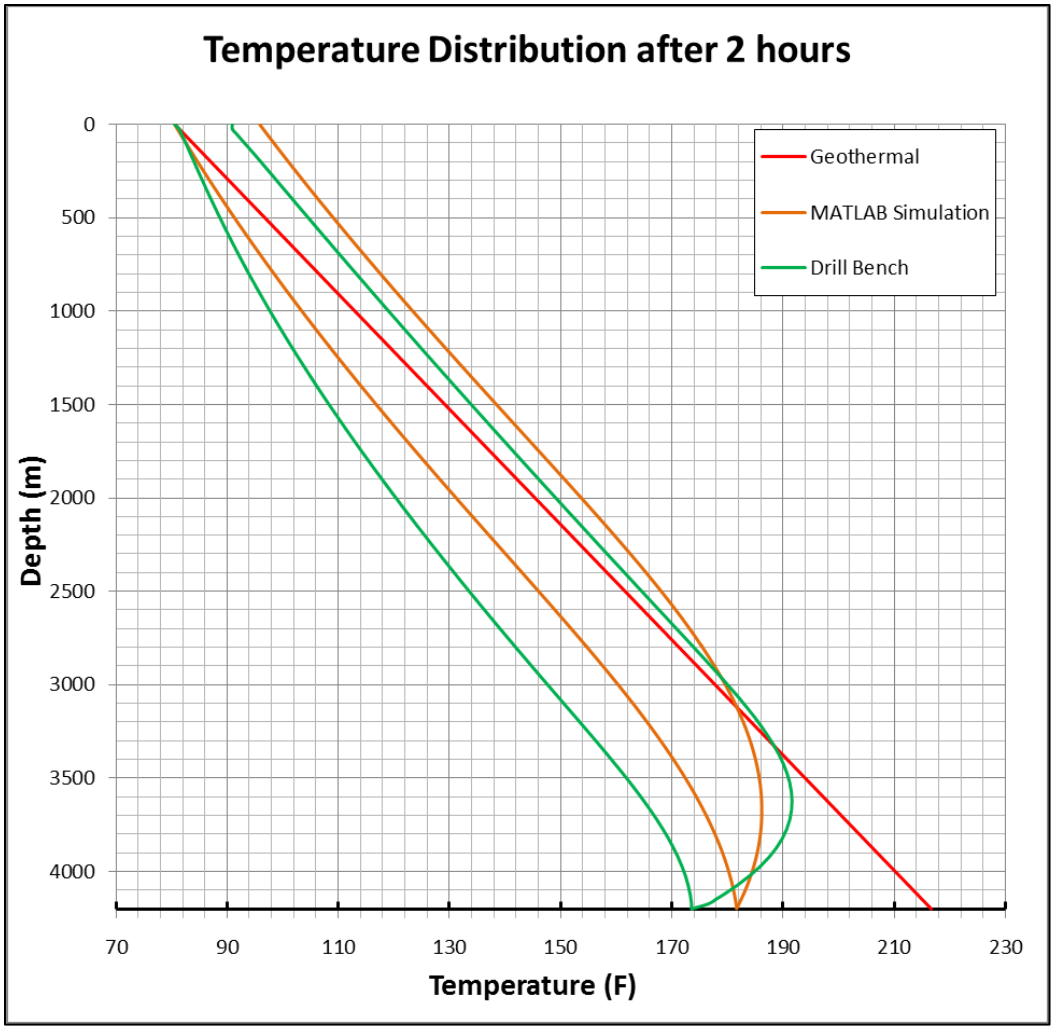

Figure 3-7: Comparison of temperature distribution after 2 hours

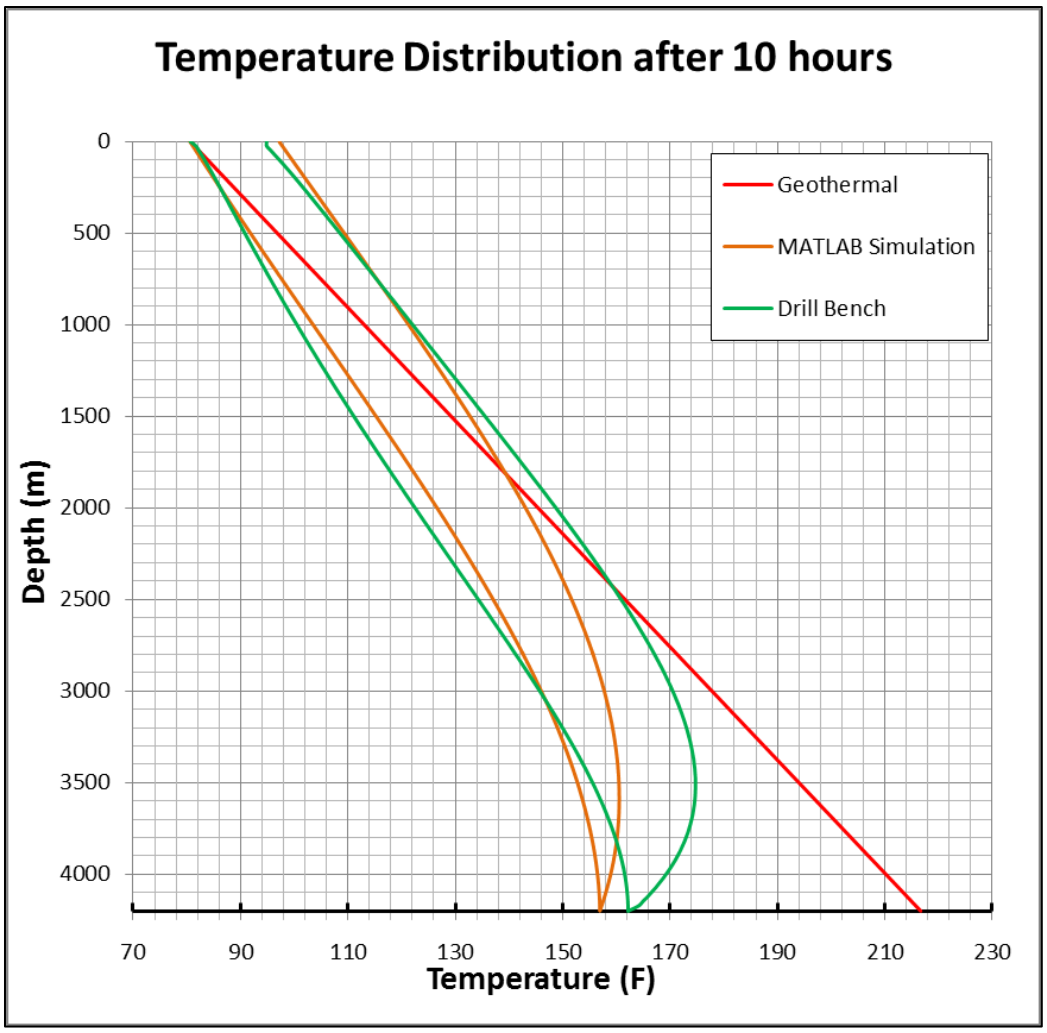

Figure 3-8: Comparison of temperature distribution after 10 hours

The difference in the transient temperature distributions at 1 and 2 hours is larger than the steady state behavior and at 10 hours. However, the trends of the two solutions are similar. The reason for the discrepancy is primarily due to the constant material property and heat transfer coefficient assumption of the simulation. There is not enough available information about some of the properties used in Drill Bench such as flow properties, heat transfer correlations and their implementations in the algorithm of the

software. Therefore, the difference between the solutions is expected up to a certain degree.

On the other hand, the fact that the results follow similar trends suggests that the results obtained from the simulation are reliable within a reasonable error margin. Moreover, the temperature distribution of the formation surrounding the wellbore is the key point for this study and the other two approaches do not include any information about formation temperature. They only serve the limited purpose of software code verification.

Chapter 4: Results and Discussion

In this chapter, the temperature distribution within the formation was presented for different heat generation scenarios. The effect of heat generation, as well as of the duration of the heat generation ware discussed. Other parameters such as fluid circulation rate also have a direct effect on the maximum temperature increase. The effects of such parameters are also presented in this chapter. Moreover, the experimental procedures for different chemical compounds used in the exothermic dissolution and the analysis of the experimental data to obtain the heat generation values were explained in this chapter.

The chapter was divided into three parts: (1) the experimental procedures to obtain the heat generation data for various compounds, (2) the temperature increase in the formation at different locations with different heat generation rates and durations, and (3) thermal stress calculations based on the temperature increase.

4.1 Heat Generation Calculation and Different Scenarios

In this study, exothermic chemical reactions were used to generate heat and increase the temperature of the formation. Different exothermic dissolutions were chosen as the chemical heat generation source. The amount of heat generated for dissolution of a particular salt is called the enthalpy of solution which depends on the crystal lattice energy and hydration energy. The total amount of heat generated depends on the enthalpy of the solution of the salt as well as the solubility of the salt in water. The amount of heat generated is limited by the saturation point of the salt. The literature values of enthalpy of solutions some salts were presented in Table 4-1.

Table 4-1: Enthalpy of Solution values of selected salts

	Molecular Weight (g/mol)	Density (g/cm^3)	Solubility @ 25C (g/100ml H_2O)	Molar Solubility @ 25C (mol/100 ml H_2O)	Enthalpy of Solution (kJ/mol)	Enthalpy of Solution (kJ/100 ml H_2O)	Added amount (g)	Dry Volume (cm^3)	Weight Ratio (%)	Volume Ratio (%)	Specific Heat Capacity (kJ/kgK)	Theoretical Temperature Increase (C)
$CaCl_2$	110.98	2.15	81.10	0.7308	20.50	14.98	150	69.77	60	41	0.6568	53.69
$CaBr_2$	199.89	3.35	143.00	0.7154	104.01	74.41	140	41.79	58	29	0.3752	154.96
$MgCl_2$	95.21	2.32	54.30	0.5703	151.88	86.62	54	23.28	35	19	0.7466	188.11
$MgBr_2$	184.11	3.72	102.00	0.5540	182.84	101.30	100	26.88	50	21	0.3802	217.96
$AlCl_3$	133.34	2.48	45.80	0.3435	325.93	111.95	45	18.15	31	15	0.6834	245.34

The enthalpy of solution for a salt can be measured using a calorimeter. Based on the literature values presented in the table, different salts were tested in the lab using a calorimeter. The temperature increase was tracked and the trend of the temperature was used to calculate heat generation values.

The experimental setup consisted of a well-insulated flask which acts like a calorimeter as shown in Figure 4-1. Three layers of insulation were used to minimize the potential heat losses. A layer of asphalt-aluminum insulation, a layer of thermal fiber insulation, and finally Styrofoam insulation were used from the inner to the outer layer. The calorimeter was placed on a magnetic stirrer to increase the speed of the reaction through agitation. Magnetic stirring also ensures the uniformity of the fluid temperature by creating turbulence within the fluid. The temperature was recorded using a Bontron temperature data logger and 4 K-type thermocouples. One thermocouple was placed in the fluid where the highest temperature increase was expected and the primary source of data for heat generation calculation. 3 other thermocouples were placed at various locations of the calorimeter to check the temperature increases other than the fluid temperature. The tracking of those temperatures was valuable for quantification or at least qualitative understanding of the heat losses which were not taken into account in heat generation calculation. One of the thermal probes was placed between the flask and the first layer of insulation, one probe was placed under the flask where there was no Styrofoam insulation and thus a possible location for heat loss, and finally one probe was placed between the thermal fiber insulation and the Styrofoam.

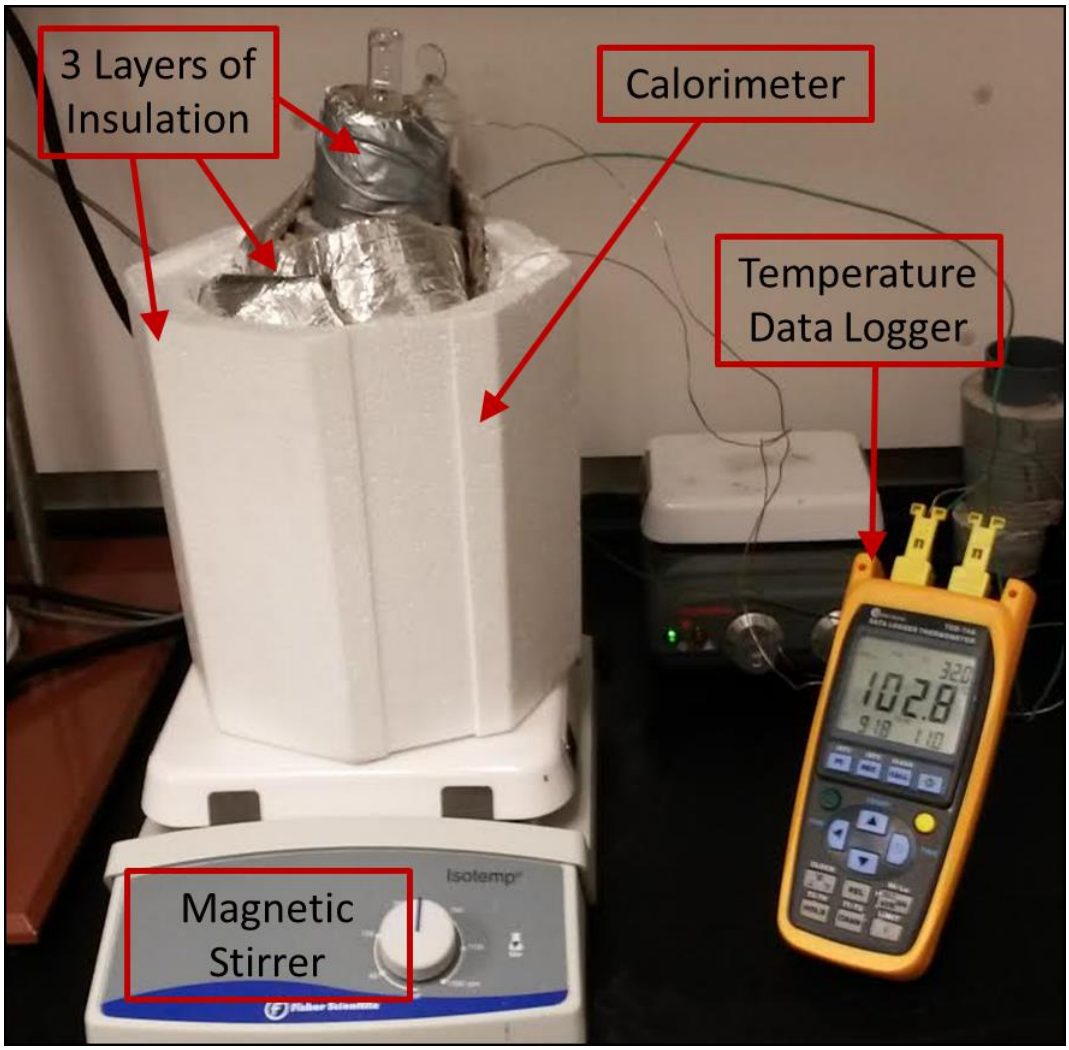

Figure 4-1: Experimental setup for enthalpy of solution measurements

As a standard procedure, for all of the experiments, same amount of water was used, namely 100 ml. For the amount of salt to be added, the solubility of the particular salt at room temperature was taken as a starting point. For some salts, the solubility in water increases considerably with temperature. Therefore the amount of salt added may exceed the solubility at room temperature to maximize the heat generation, since the hotter water can dissolve more of the salt.

The temperature of the fluid was recorded as the salt was being added. The addition rate of salt was crucial as slow rates of addition result in considerable heat losses. However, for some compounds the reaction was rather violent and the addition rate was kept slow for safety purposes. The Figures 4-2 to 4-6 show the temperature plot of some of the experiments.

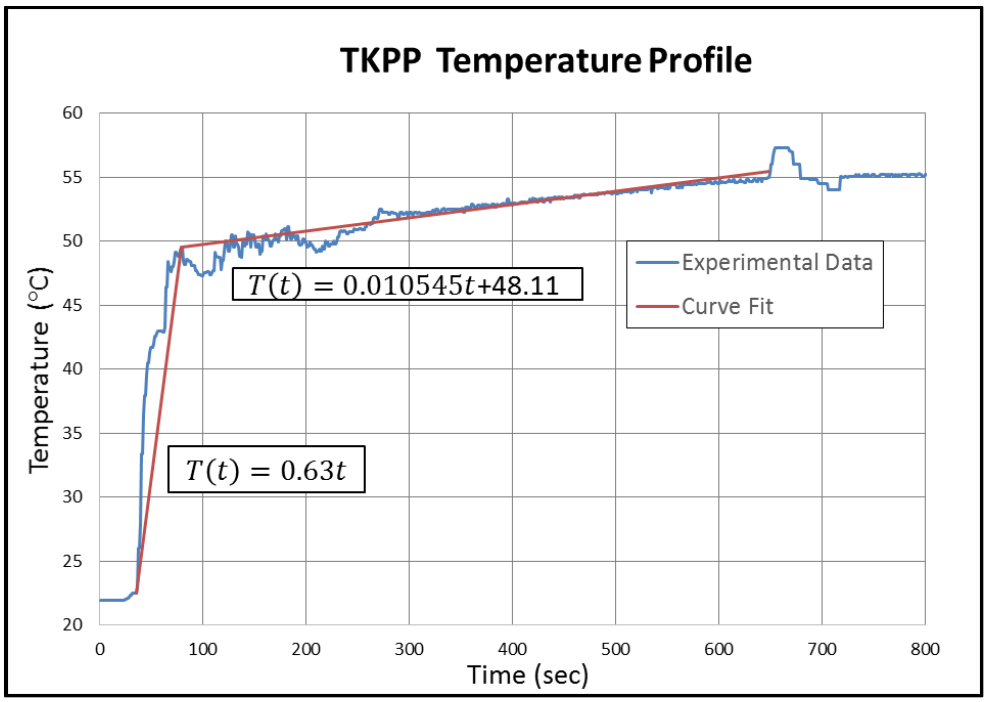

Figure 4-2: Fluid temperature increase for tetra potassium pyrophosphate ($K_4P_2O_7$, TKPP)

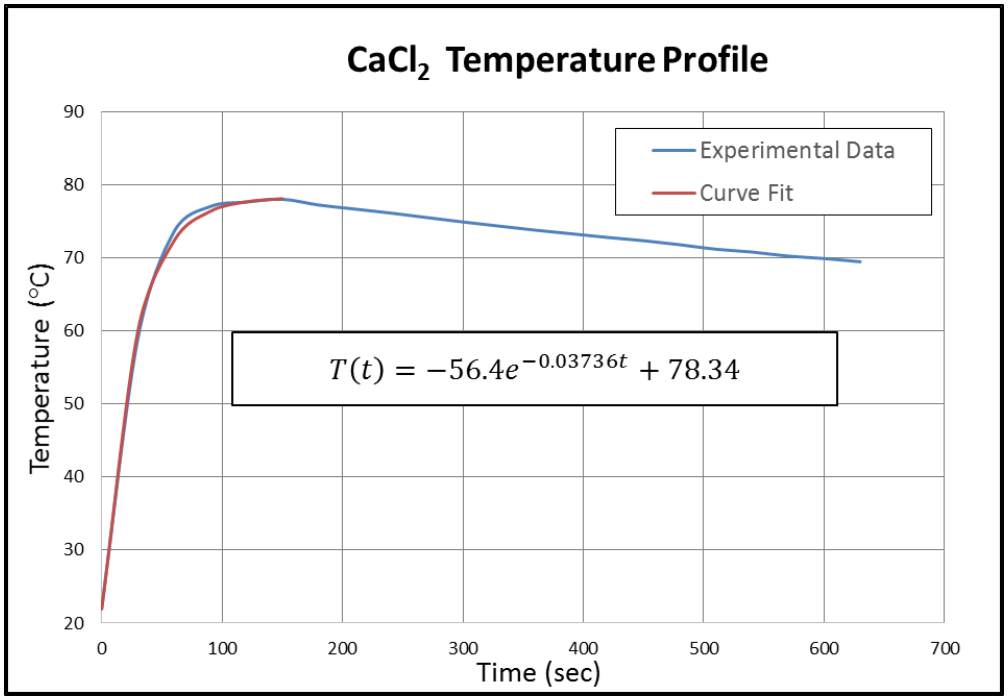

Figure 4-3: Fluid temperature increase for CaCl2

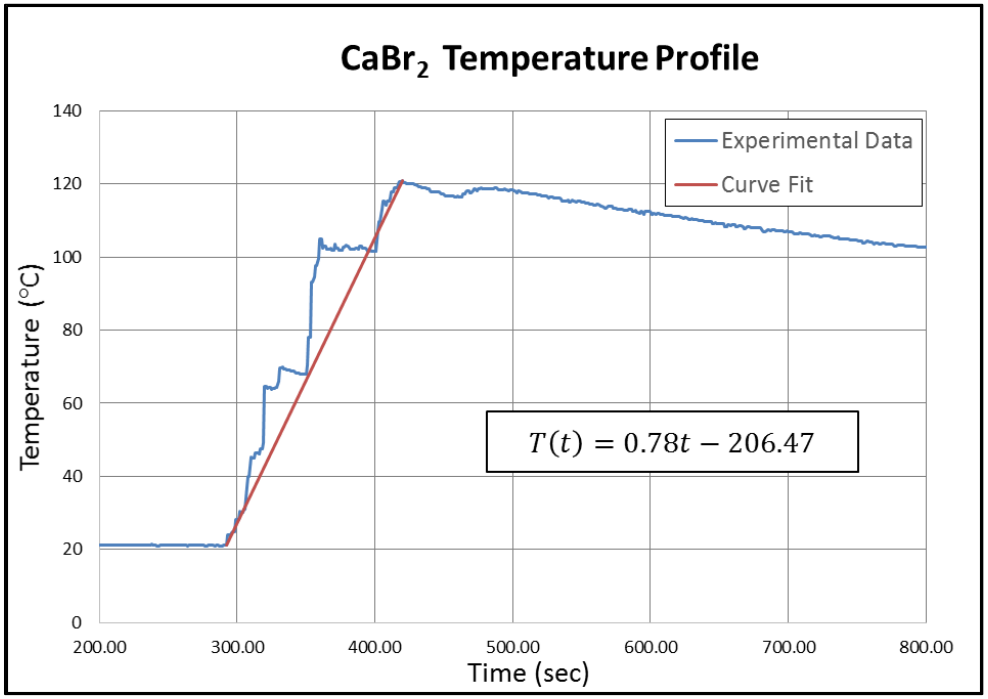

Figure 4-4: Fluid temperature increase for $CaBr_2$

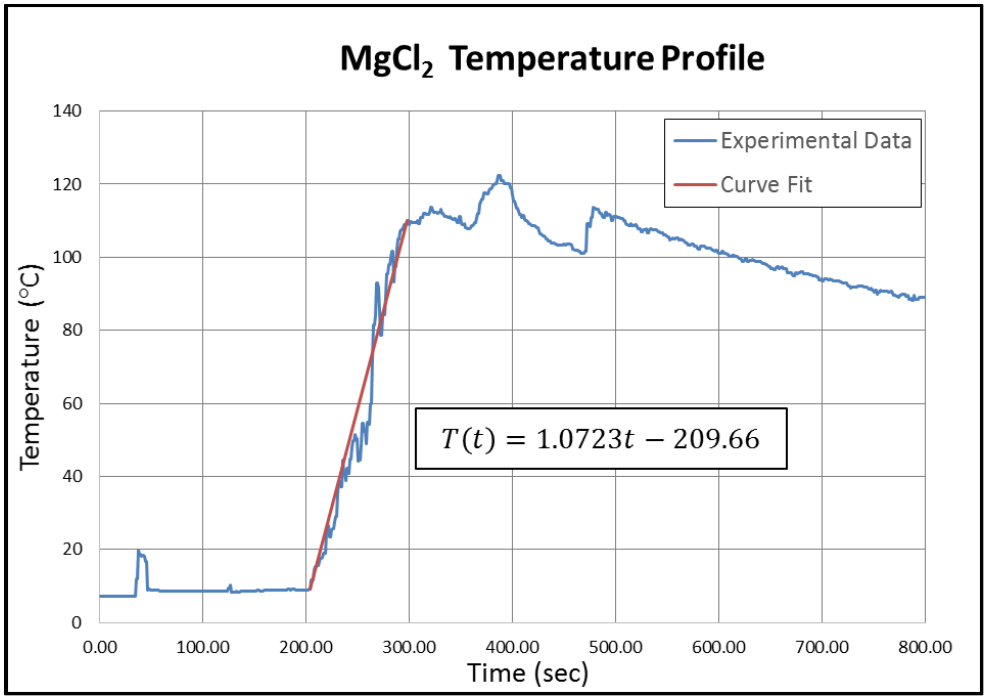

Figure 4-5: Fluid temperature increase for $MgCl_2$

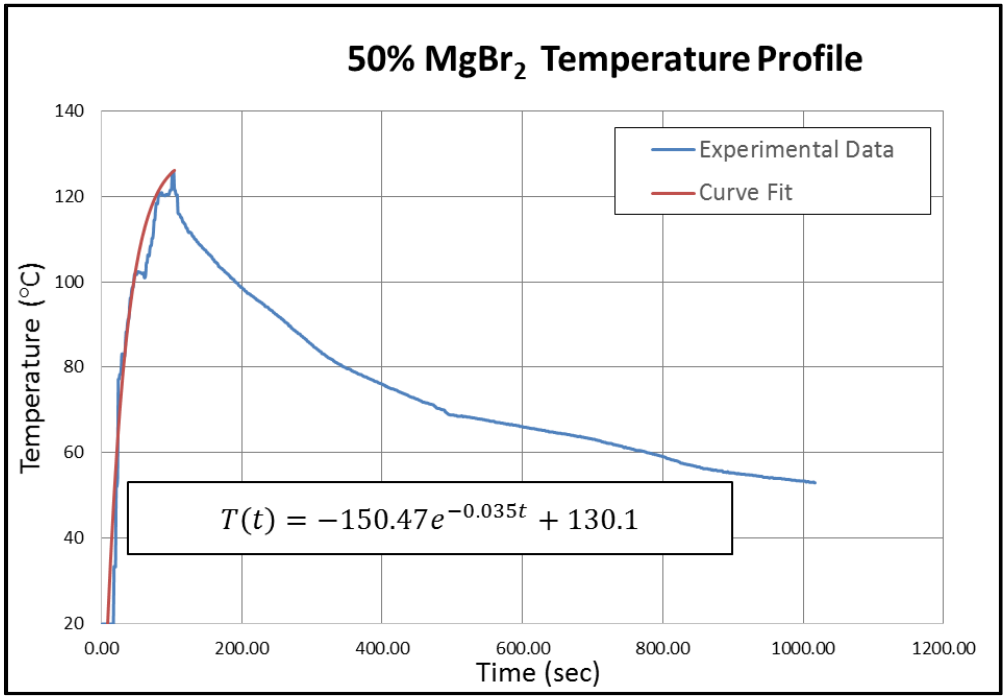

Figure 4-6: Fluid temperature increase for $MgBr_2$

The temperature increase profiles of the selected salts were then analyzed for heat generation calculation. As shown in the previous figures, a curve was fit to the experimental data. The mathematical representation of the temperature increase was used to calculate according to the following formula.

$$\dot{Q}_{gen} = \rho c \frac{dT}{dt} \tag{4.1}$$

This calculation was based on the assumption that there was no heat exchange between the fluid and the surroundings and all the heat generated during the chemical reaction was stored in the water. This assumption makes the calculation of the heat generation conservative for two reasons: (1) the calorimeter was not perfectly insulated and the heat loss was not zero, and (2) some of the generated heat was stored in the salt, flask, insulation etc. Therefore the actual heat generation was slightly higher than the calculated heat generation.

Similar experiments were conducted with the delayed and extended reaction. One crucial difference between the actual dissolution and the delayed dissolution experiments was the fact that when the duration of the experiment was extended, the error due to heat loss increased significantly. The "adiabatic calorimeter" assumption depends on the duration of the processes and this assumption may not be a good assumption for delayed reactions.

Figure 4-7 below shows the temperature profile of $CaCl_2$ in a delayed reaction test. The highest fluid temperature achieved was significantly lower than the reaction without any delay.

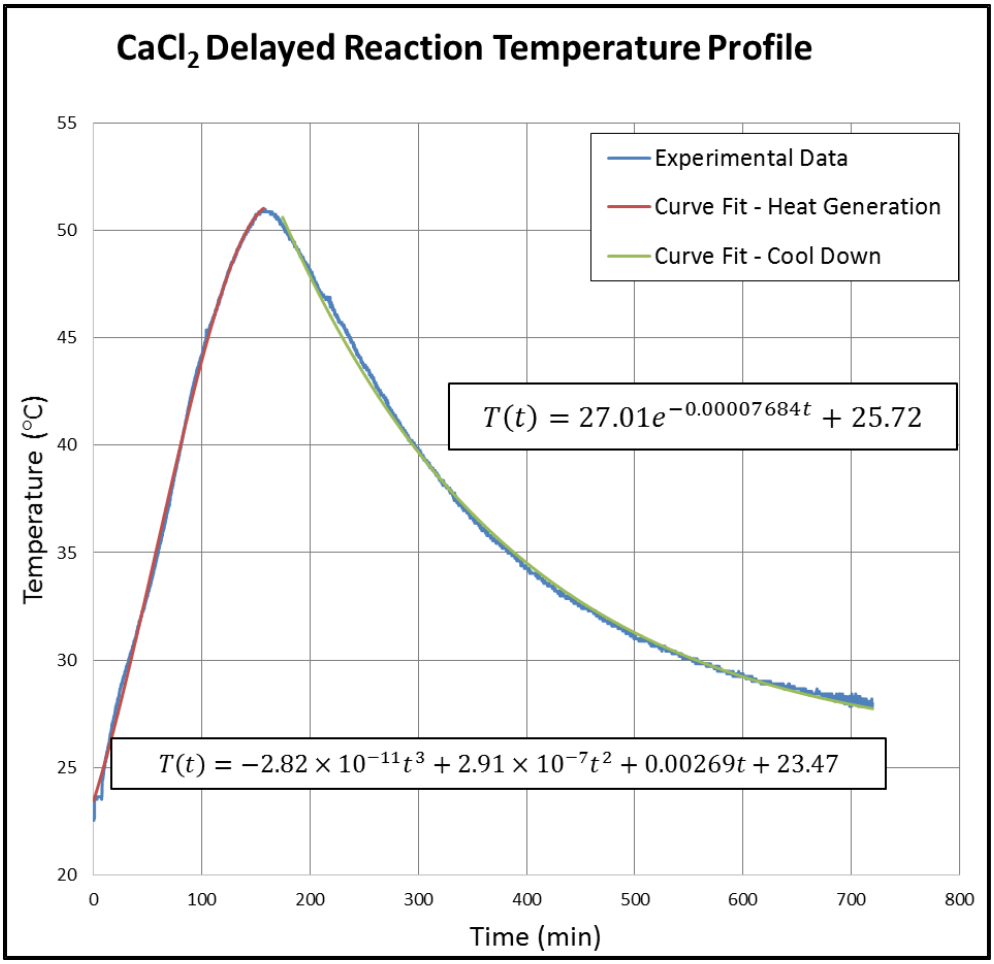

Figure 4-7: Fluid temperature profile for $CaCl_2$ in delayed reaction

Ideally, if there was no heat loss, the highest temperature of fast and slow reactions would be the same. The major reason of the lower final temperature was the loss of accuracy in calculating enthalpy of solution due to heat losses. One other reason for the difference between the two experiments may be the additional thermal mass of the materials that delay the reaction which decreases the temperature increase for the same amount of heat generation. Since all the generated heat was assumed to be in the water, this can be considered as another experimental error. Finally, the chemistry that drives the dissolution may be affected by the materials that retard the reaction. However, they

were chosen to be inert particles for this chemical reaction, and they are insoluble in water. Therefore, it is unlikely that the solubility of the salt was affected due to these particles.

In Figure 4-8, the ideal temperature and heat generation profiles were graphed for different reaction rates. Since the total amount of energy that can be released from the salt depends only on the enthalpy of the solution and the solubility, the final temperature of the fluid must be same for different reaction rates. For faster reactions, higher heat generation is maintained for a shorter time period whereas for slower reactions the heat generation rate is lower but lasts for longer periods. This keeps the area under the heat generation curve the same since it represents total heat release.

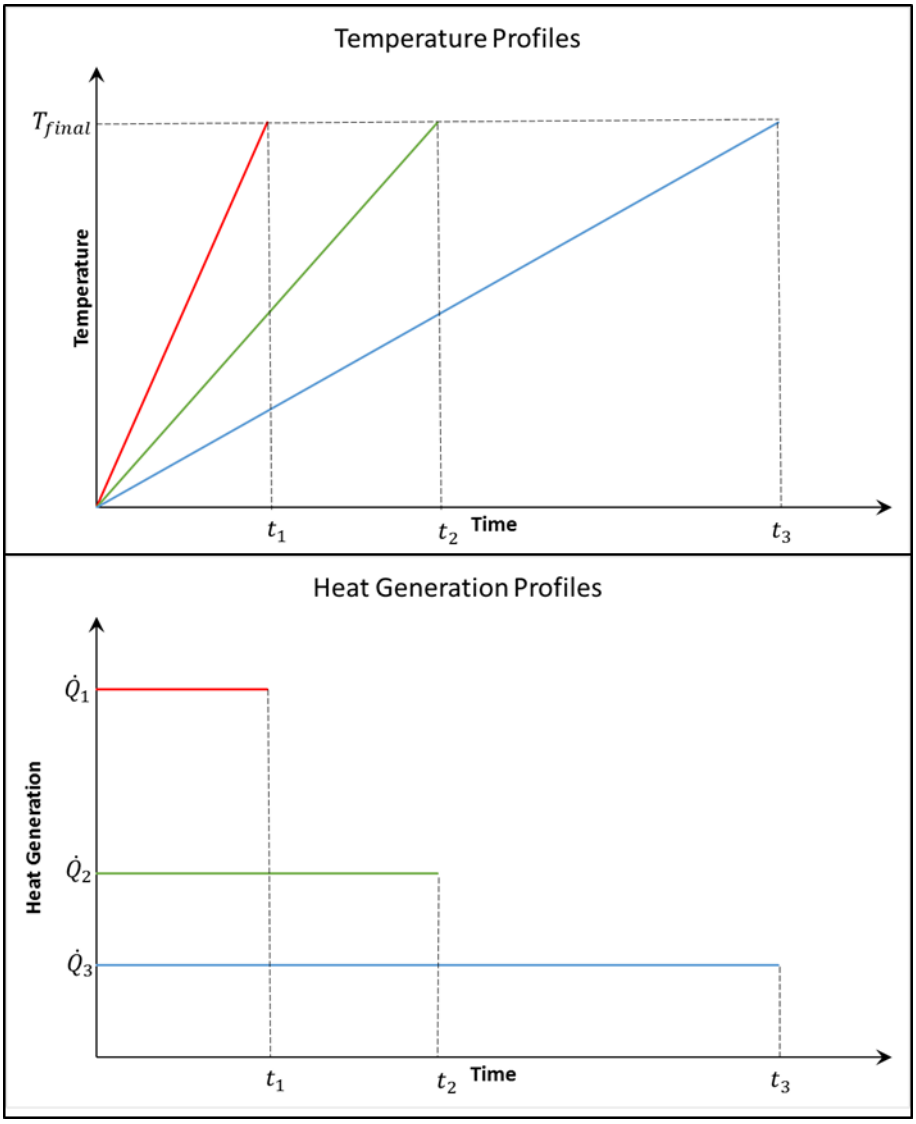

Figure 4-8: In the ideal case temperature and heat generation profiles for different reaction speeds

As discussed before, the reason that this behavior was not seen in the experimental results is the fact that for slower reactions heat loss was more significant. However, in the actual application, this is not a problem because the heat will be lost to surrounding environment which is the formation. This is in fact the ultimate goal. Therefore, for further analyses, the experimental results from the fast reactions were used

as they represent the actual heat generation more accurately due to lower experimental heat losses. To investigate the effects of different heat generation rates, the heat generation and the duration of the heat generation was adjusted accordingly such that the total heat release was kept same as the experimental results for the fast reactions.

A secondary effect of the heat generation rate and the heat generation duration is on the circulation rate of the fluid. In order to maximize the heat transfer to the target zone of the formation, the heat generation duration must match the travel time of the reactive fluid along the target zone. Fast circulation rates may cause reactive fluid to be carried away before it releases all of its chemical energy. On the other hand, slower circulation rates may cause all the heat to be released before covering the entire target zone. Therefore, the circulation rate needs to be optimized for the maximum heat transfer to the formation.

The circulation rate affects heat transfer also via the heat transfer coefficient. The velocity of the fluid within the casing and also in the annulus determines the heat transfer coefficient between the fluid inside the casing and in the annulus, and the fluid in the annulus and the formation, respectively.

The effect of circulation rate was discussed later in this chapter.

4.2 Temperature Distribution For Different Heat Generation Scenarios

Based on the experimental heat generation data, different values of heat generation and heat generation duration were implemented using the computational model. Figure 4-9 shows the diagram of the problem with a real case geometry for Mars B field application, heating rock prior to cementing.

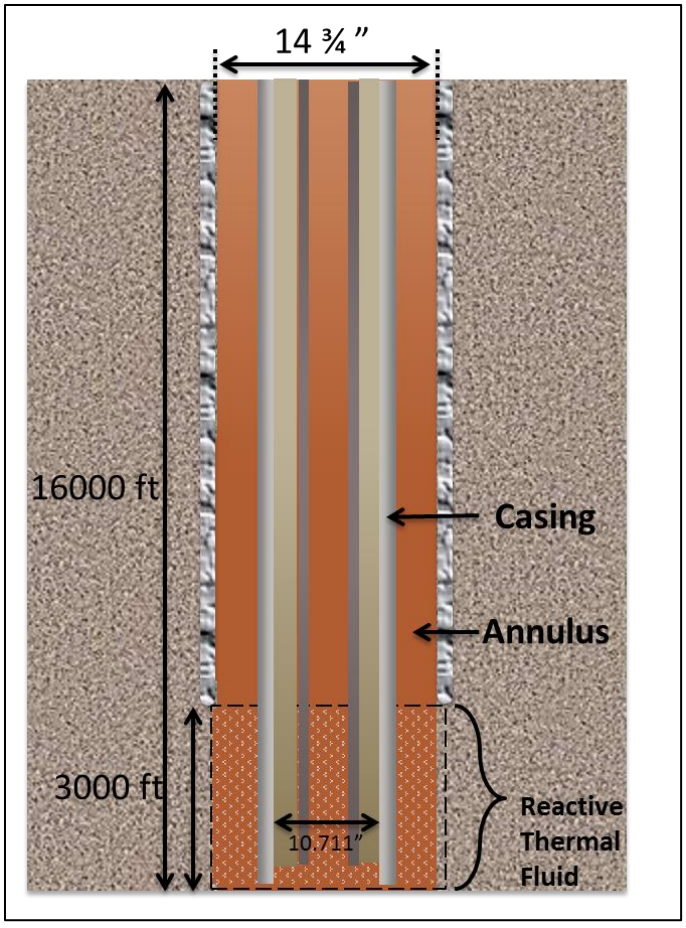

Figure 4-9: Diagram of the problem

The parameters used in the calculations are shown in Table 4-3.

Table 4-2: Calculation Parameters

Geometry				
Casing OD	0.3016	m	11 7/8	in
Casing ID	0.2721	m	10.711	in
Annulus Clearance	0.03651	m	1.4375	in
Far field distance	0.5	m	1.64	ft
Depth	4877	m	16000	ft

Material Properties			
	Density (kg/m^3)	Specific Heat Capacity (kJ/kgK)	Thermal Conductivity (W/mK)
Fluid	1384	2500	1.02
Casing	7840	800	50
Formation	2500	1200	2.2

Other Parameters				
Circulation Rate	14	kg/s	160	gal/min
Injection Temperature	4.44	°C	40	°F
Surface Temperature	4.44	°C	40	°F
Temperature Gradient	0.01434	°C	0.00787	°F/ft

The simulation was run first for the conventional circulation case of circulating "the long way". In order to obtain the initial temperature distribution, the simulation ran for a certain amount of time without heat generation, circulating the fluid, and cooling the

formation. The temperature distribution obtained at this point was assumed to be the initial temperature distribution for all media. At that point, heat generation started at the bottom of the well both in the casing and in the annulus at the same time with the specified rate and continued for a certain amount of time. After the heat generation stopped, so does the circulation to allow heat transfer between the formation and the hot fluid. Otherwise, the high temperature region in the fluid travels up with the flow velocity.

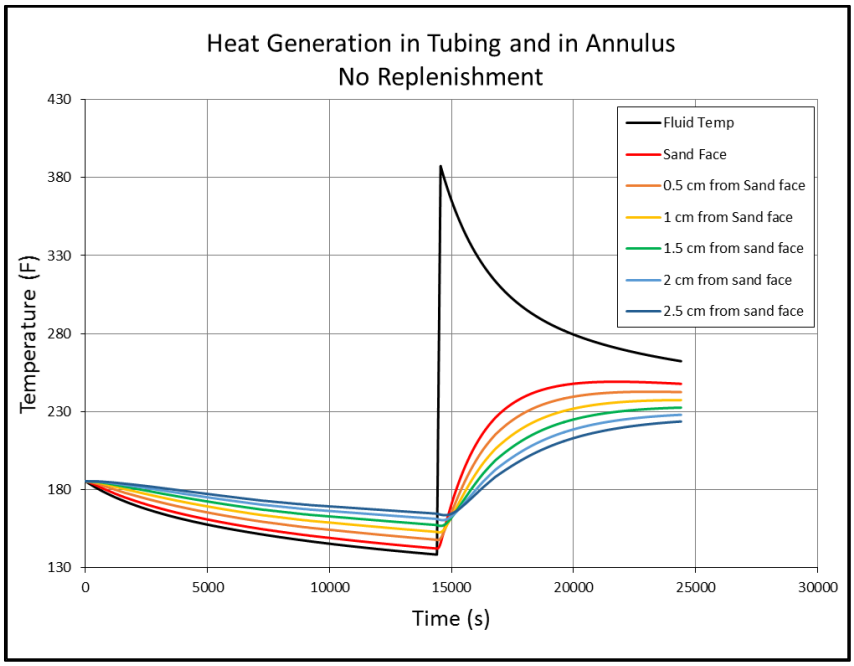

Figure 4-10: Temperature history at various locations for high heat generation

First, heat generation was assumed to be as high as the reaction without any delay. The duration of the reaction was on the order of minutes. The data was taken from experimental results. The heat generation was taken to be 3,250 W/m^3, and it lasted for 140 seconds. The circulation rate was taken to be zero after the reaction started. In other

words, the exothermic materials reach the target zone and the reaction starts there immediately.

Figure 4-10 shows the temperature history of the fluid temperature and various locations inside the formation, at the bottom hole location. The temperatures go down first because of mud circulation. As the materials react almost instantaneously, the fluid temperature increases within a very short time, from about 138 °F to 387 °F. As expected, the response of the formation was rather slow. The time it requires to reach the maximum temperature inside the formation was on the order of hours. The temperature at 0.5 cm from the sand face increased from about 150 °F to 240 °F with an increase about 90 °F.

Note that this case imitates the experimental conditions, by having a high heat generation rate and short heat generation time. However, since it requires some time to deliver the particles to the target zone, the reaction needs to be delayed for a certain amount of time so that the heat loss is minimized. Because of the retardation mechanism the heat generation will be decreased as the generation time is extended, keeping the total amount of energy produced the same. Next, a lower heat generation was assumed with extended duration.

The heat generation rate was now assumed to be 10 times less with reaction lasting 10 times longer. Namely, one single particle will generate heat for 1400 s at a rate of 325 kW/m^3. The circulation rate was chosen such that the travel time of one particle through the drill pipe and back up in the annulus, along the target zone coincides with the total reaction time, i.e.1400 s. As discussed before, faster circulation rates would cause reactive particles to be carried away when they still have the potential to generate heat. On the contrary, slower heat generation rates would cause heat generation to stop before particles cover the entire target zone.

After the optimum circulation rate was chosen, it was possible to continue circulation as long as the operational criteria allow. As the replenishing continues, it is possible to transfer larger amounts of energy in the form of heat to the formation.

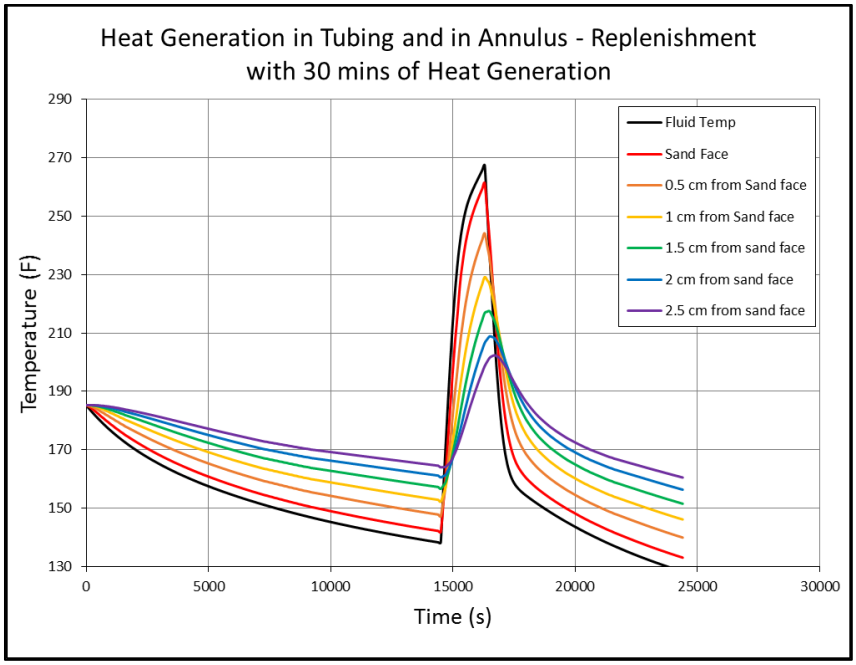

Figure 4-11: Temperature history at various locations for heat generation rate of 325 kW/m^3 and replenishing of 30 minutes

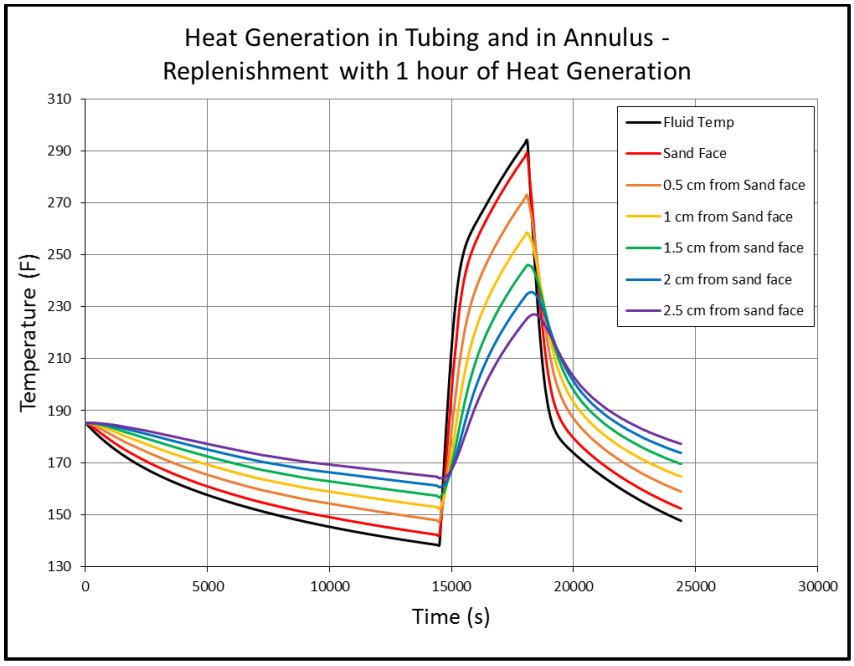

Figure 4-12: Temperature history at various locations for heat generation rate of 325 kW/m^3 and replenishing of 1 hour

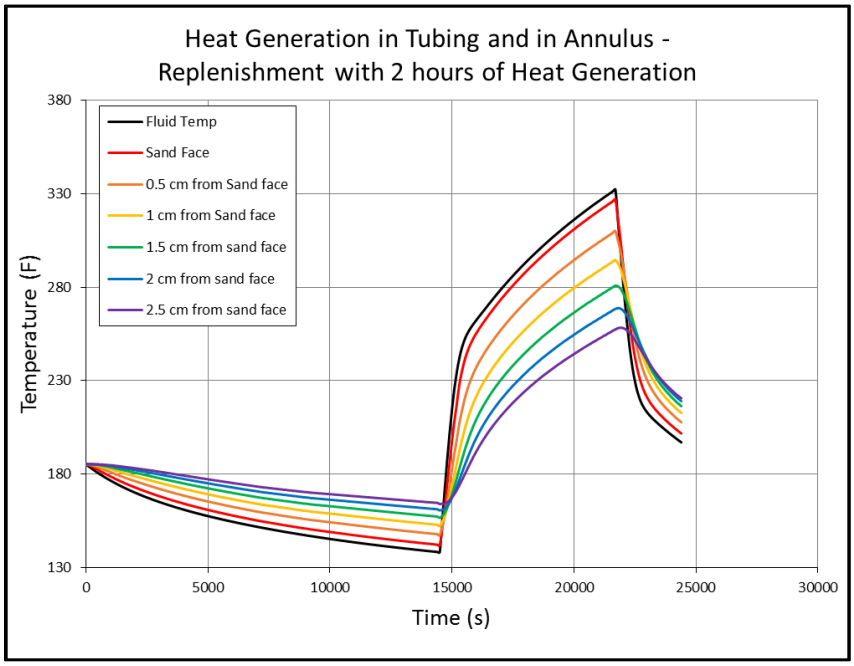

Figure 4-13: Temperature histories at various locations for heat generation rate of 325 kW/m^3 and replenishing of 2 hours

Figures 4-11, 12, and 13 show the temperature history of various locations as well as the fluid temperatures at the bottom hole location. As expected, with longer replenishment times the maximum temperature both for fluid and for the formation increases. For all of the cases, initial temperature at 0.5 cm deep was around 150 °F, just like the previous case. The highest temperature at the same location was calculated to be 244 °F, 273 °F and 309 °F for 30 minutes, 1 hour and 2 hours of replenishment, respectively. The temperature increase was calculated to be 94 °F, 123 °F, and 159 °F, respectively.

A similar analysis can be done with even lower heat generation rates by adjusting the reaction time accordingly so that the total energy produced by any particle is kept the same. Figures 4-14 to 4-19 show the temperature histories for heat generations of 250 kW/m^3 and 100 kW/m^3, and three different replenishment times.

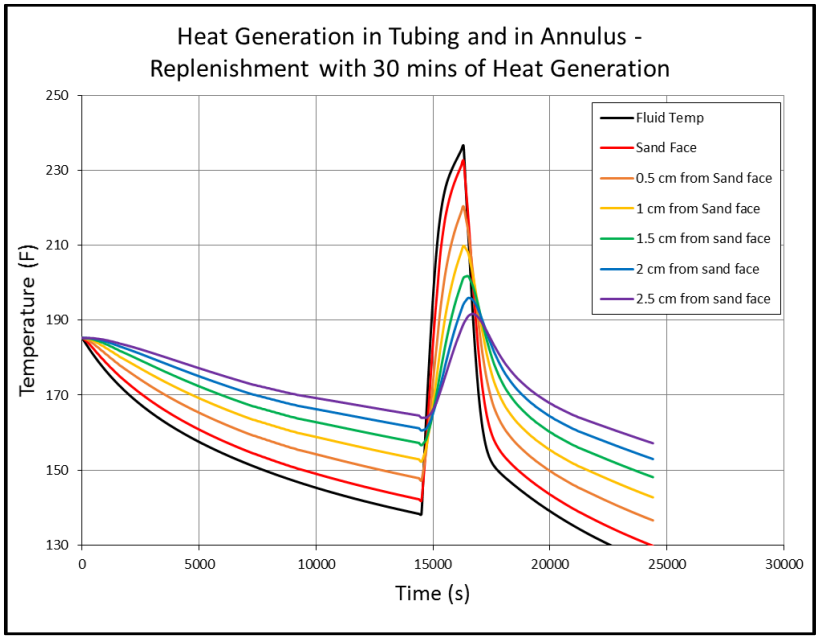

Figure 4-14: Temperature history at various locations for heat generation rate of 250 kW/m^3 and replenishing of 30 minutes

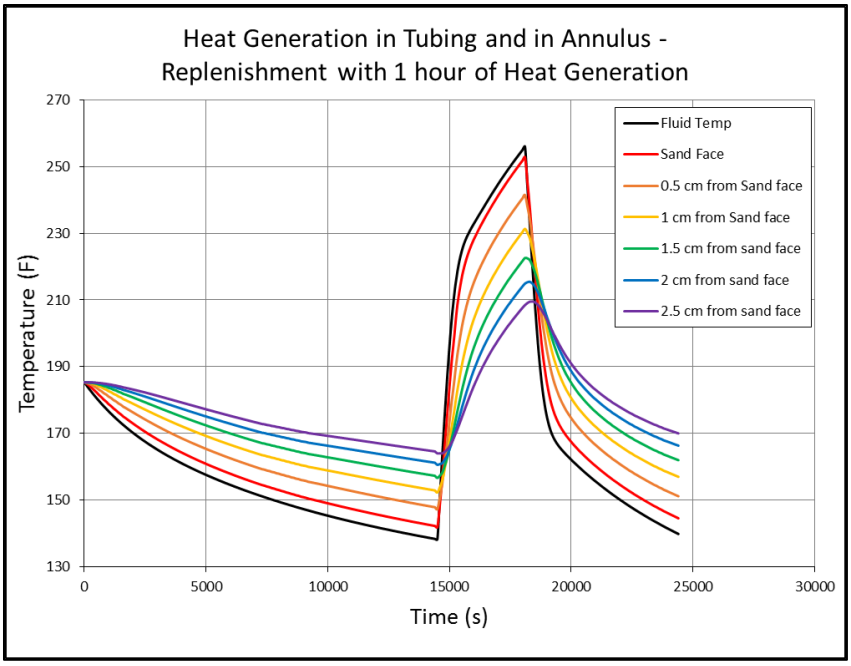

Figure 4-15: Temperature history at various locations for heat generation rate of 250 kW/m^3 and replenishing of 1 hour

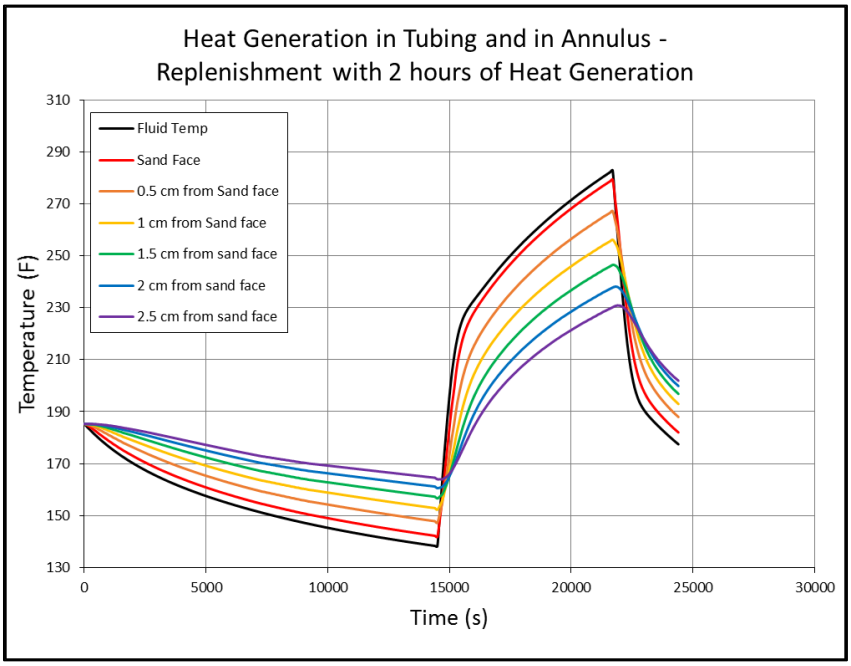

Figure 4-16: Temperature history at various locations for heat generation rate of 250 kW/m^3 and replenishing of 2 hours

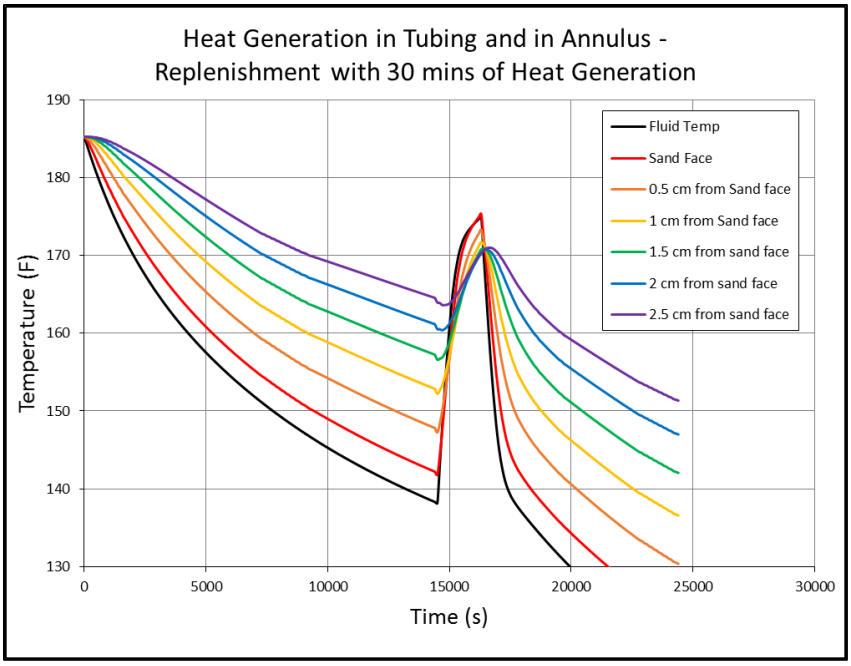

Figure 4-17: Temperature history at various locations for heat generation rate of 100 kW/m^3 and replenishing of 30 minutes

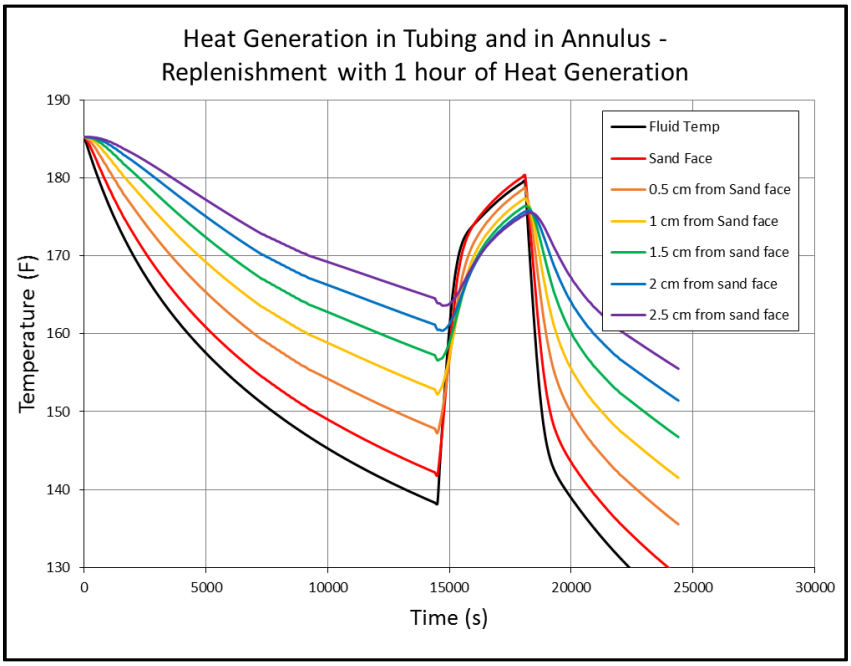

Figure 4-18: Temperature history at various locations for heat generation rate of 100 kW/m^3 and replenishing of 1 hour

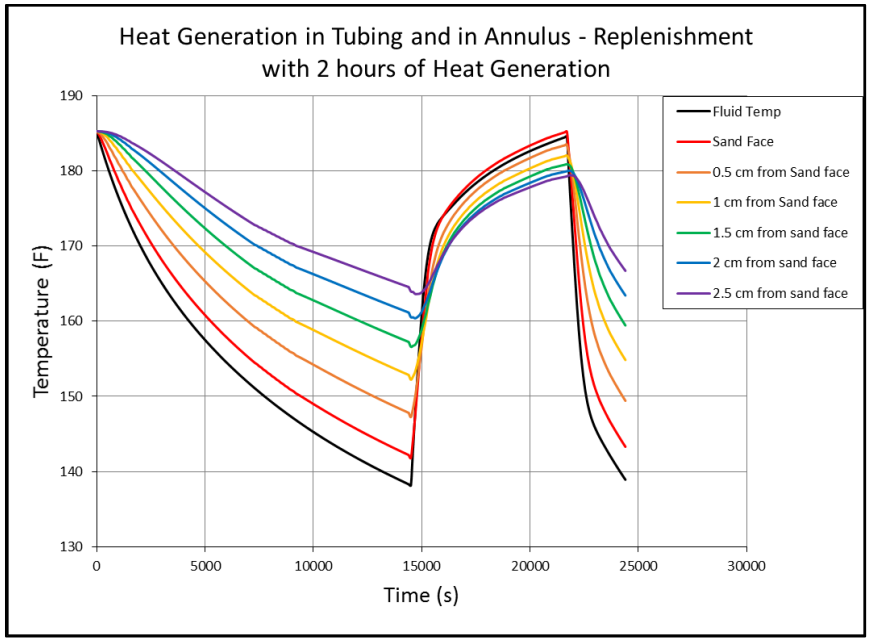

Figure 4-19: Temperature history at various locations for heat generation rate of 100 kW/m^3 and replenishing of 2 hours

The temperature histories indicate that for lower heat generation rates result in lower temperature increases as expected. For 250 kW/m^3 of heat generation the temperature increased at the same location 70 °F, 91 °F, and 116 °F for 30 minutes, 1 hour, and 2 hours of replenishment. For 100 kW/m^3 of heat generation rate, the temperature rose 26 °F, 31 °F, and 36 °F at the same location.

It is noteworthy that for the last two heat generation rates, the reaction lasts longer than the first heat generation rate since the reaction is delayed longer. Therefore, the circulation rate which was optimum for a heat generation rate of 325 kW/m^3 is no longer the optimum circulation rate for the other two cases. Since the reaction is slower, the circulation rate must be slower as well, to allow for the heat generation to be completed before the fluid is carried away.

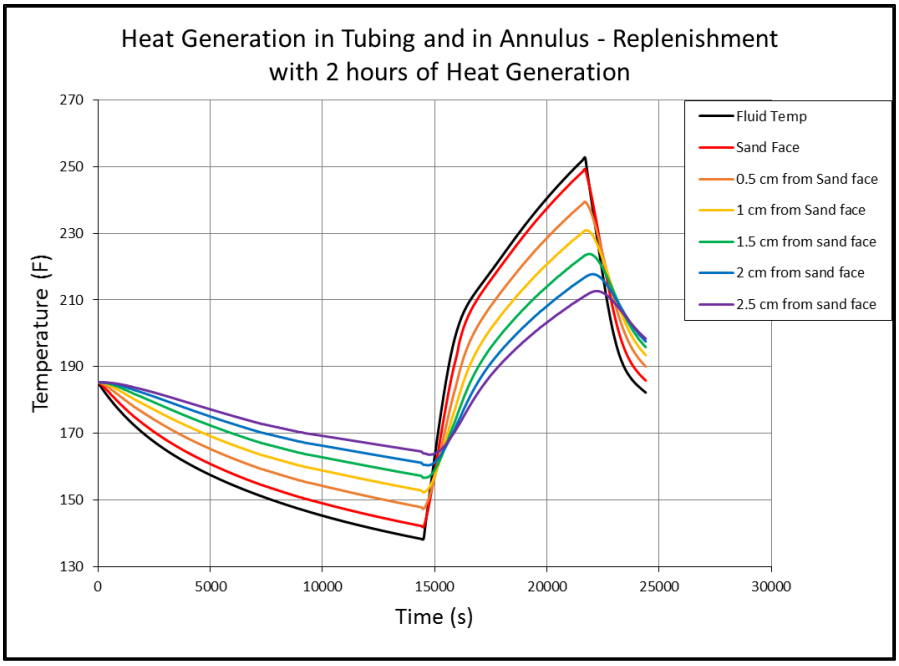

Figure 4-20: Temperature history at various locations for heat generation rate of 100 kW/m^3 and replenishing of 2 hours with slow circulation

Figure 4-20 shows the same case as Figure 4-18, except for slower circulation rate. Circulation rate was slowed down to match the slower reaction rate. The temperature increased at 0.5 cm depth from the sand face by 92 °F, whereas for the same reaction rate and replenishment time, it increased only 36 °F for fast circulation rate.

4.3 Using Temperature Distribution For Thermal Stress Calculation

Thermal stress calculations based on temperature increases require detailed analyses, since the temperature increase within the rock is a function of time, and it is not uniform in the radial direction. Zoback (Zoback et al. 2003) suggests that the thermal component of the tangential stress can be estimated for steady state with equation 4.2.

$$\sigma_{\theta\theta}^{\Delta T} = \frac{\alpha_t E \Delta T}{(1-\nu)} \tag{4.2}$$

Although calculation of thermal stress requires dynamic stress modeling, equation 4.2 is still useful in order to calculate the order of magnitude of the thermal stresses.

Table 4-4 shows thermo-elastic properties of selected formations characteristic of Mars B well applications. The data was supplied by Shell Geomechanics group.

Table 4-3: Thermo-elastic properties of rock formations

Formation	Lab name	Sample Depth, ft	Vertical stress, psi	Minimum horizontal stress, psi	Young's modulus, kpsi	Poisson ratio	Thermal Expansion Coefficient (1/K)
E2	Pink	11775	2045	369	250	0.3	0.0000062
Above H1	Above Orange	14276	2060	399	354	0.13	0.0000062
M1,M2 (L1,L2)	Upper Green	not known	not known	not known	228-263	0.13-0.27	0.0000062
	Ursa shale	18756	2120	144	410	0.16	0.0000062

For these formations, the steady state thermal stress changes with the increase in the temperature are shown in Figure 4-21.

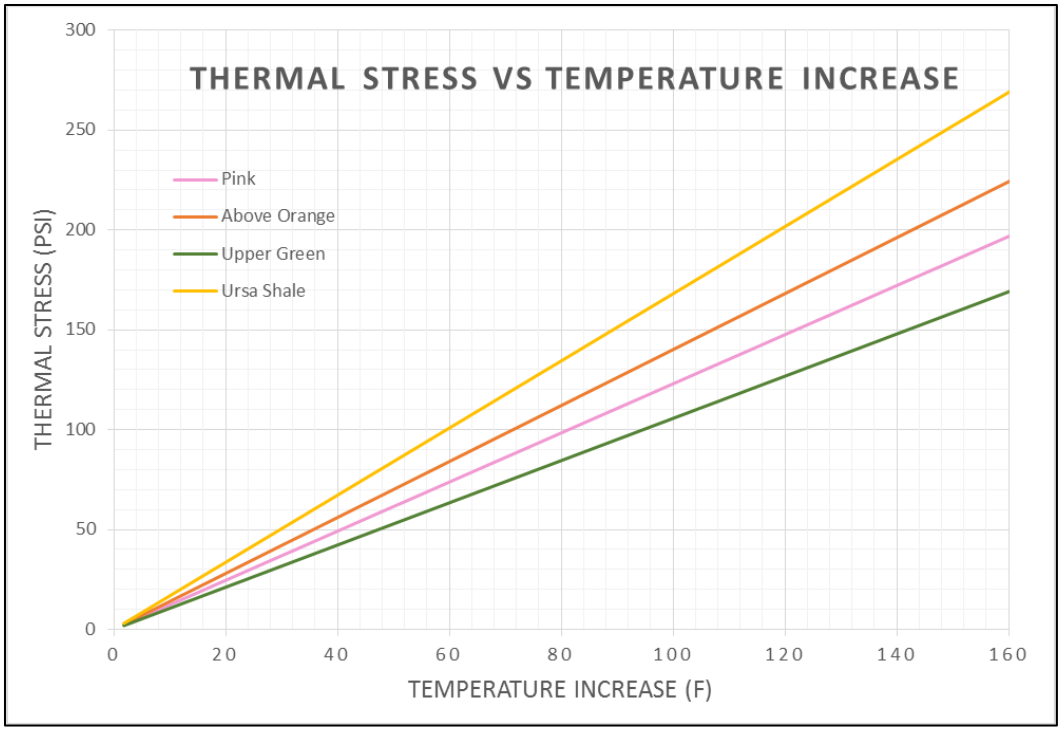

Figure 4-21: Thermal stress vs temperature increase for 4 different formations

The temperature increase in the formation, at 0.5 cm from the sand face, changes from 100 °F to 160 °F depending on the heat generation rate, replenishment time, circulation rate etc. For 100 °F temperature increase, the thermal stress ranges between 100 psi for Upper Green formation to 170 psi for Ursa Shale. For 160 °F temperature increase, the thermal stress ranges between 170 psi for Upper Green to 270 psi for Ursa Shale.

For most of the cases, temperature increase is not uniform but a function of radial distance. For non-uniform temperature increase, thermal stress can be written in the following form (Tang & Luo 1998):

$$\sigma_r = -\frac{\alpha E}{(1-\nu)}\frac{1}{r^2}\int_{r_w}^{r} r\Delta T dr \tag{4.3}$$

$$\sigma_\theta = -\frac{\alpha E}{(1-\nu)}\frac{1}{r^2}\left[\int_{r_w}^{r} r\Delta T dr - r^2\Delta T\right] \tag{4.4}$$

$$\sigma_z = -\frac{\alpha E}{(1-\nu)}\Delta T \tag{4.5}$$

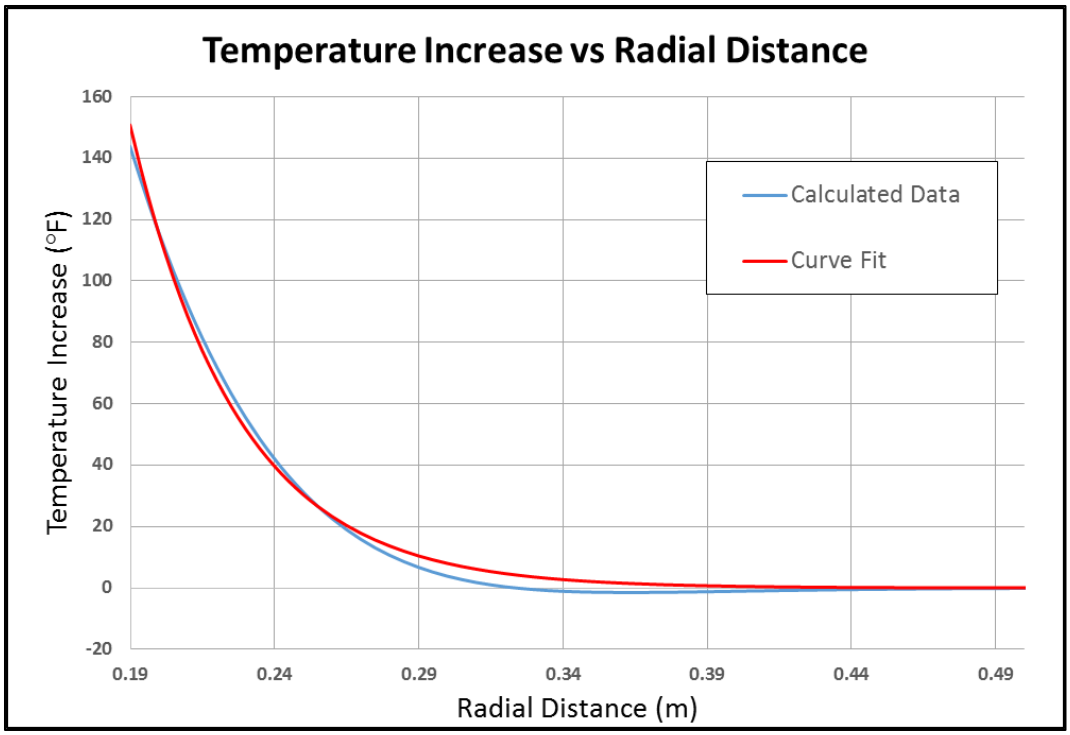

Figure 4-22: Temperature increase with respect to radial distance when the highest temperature is reached

Figure 4-22 shows the distribution of temperature increase when the highest temperature increase for 325 kW/m^3 and 2 hours of replenishment which was shown in Figure 4-13. Temperature increase exponential decaying trend which can be represented as $\Delta T = ae^{-br}$. For that particular case a is calculated to be 13220 and b is 26.66. Along with this representation, equation 4.4 for tangential stress can be evaluated analytically.

$$\sigma_\theta = -\frac{\alpha E}{(1-\nu)}\frac{1}{r^2}\left[\int_{r_w}^{r} rae^{-br}dr - r^2 ae^{-br}\right] \tag{4.6}$$

$$\sigma_\theta = -\frac{\alpha E}{(1-\nu)}\frac{1}{r^2}\left[-\frac{a}{b}re^{-br}\Big|_{r_w}^{r} + \int_{r_w}^{r}\frac{a}{b}e^{-br}dr - r^2 ae^{-br}\right] \tag{4.7}$$

$$\sigma_\theta = -\frac{\alpha E}{(1-\nu)}\frac{1}{r^2}\left[-\frac{a}{b}re^{-br}\Big|_{r_w}^{r} - \frac{a}{b^2}e^{-br}\Big|_{r_w}^{r} - r^2 ae^{-br}\right] \tag{4.8}$$

$$\sigma_\theta = -\frac{\alpha E}{(1-\nu)}\frac{1}{r^2}\left[-\frac{a}{b}e^{-br}\left(r+\frac{1}{b}\right)\Big|_{r_w}^{r} - r^2 ae^{-br}\right] \tag{4.9}$$

Using equation 4.9, tangential stress due to temperature increase can be plotted as a function of radial distance as in Figure 4.23.

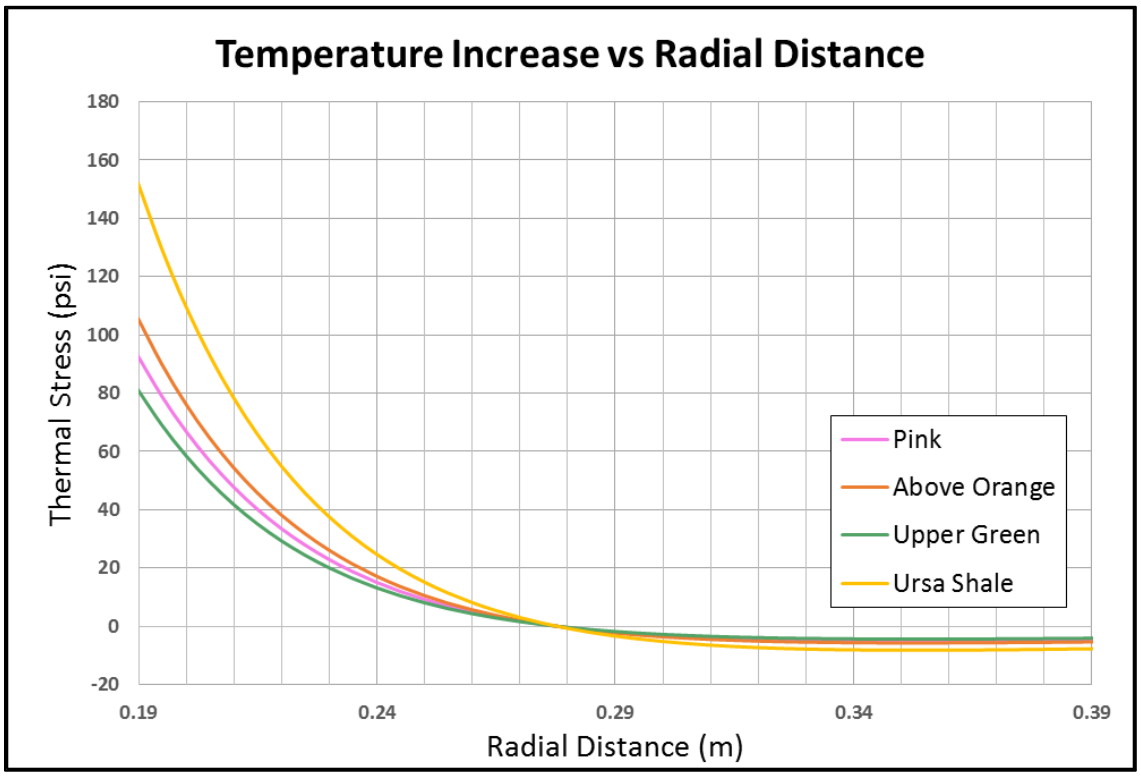

Figure 4-23: Thermal stress as a function of radial distance for non-uniform temperature increase

Chapter 5: Conclusion and Future Work

This chapter discusses the results of different heat generation cases in terms of temperature distribution and thermal stresses. Some improvements to the model and thermal stress calculations were suggested here for future work.

5.1 CONCLUSIONS

It was seen that the temperature distribution of the formation in the close vicinity of the wellbore can be increased on the order of 100 °F which in return introduces thermal stress on the order of 100 psi in the formation depending on the material properties of the formations. The increase in the thermal stresses can be engineered in a way such that the fracture gradient is increased to maintain wellbore stability and strength to decrease risk of the lost circulation and improve cement job.

Various chemical compounds were tested at standard conditions and the heat generation rates of each candidate were investigated under different conditions, for different carrier fluid as well as pure water. The temperature increase for a thermally isolated calorimeter ranged from 90 °F to 220 °F. The highest temperature increases were achieved with $CaBr_2$, $MgCl_2$ and $MgBr_2$. Because of ease of procurement, $MgCl_2$ was chosen for detailed experiments. The experiments with uncoated particles were consistent both in terms of highest temperature achieved and the heat generation rate. Various different coating methods were used to achieve the desired delay effect on the kinetics of the reaction. Although the experiments with the coated particles were useful in order to evaluate the delay of the reaction, in terms of heat generation calculations, the accuracy of those experiments was questionable since the heat loss was a considerable source of error for extended reaction times. The highest temperature achieved with the coated particles was significantly less than that of the uncoated particles. This indicates the

excessive heat loss to the surrounding, since the temperature increase is expected to be the same for different reaction rates assuming perfect insulation. Therefore, in order to model the heat generation from coated particles, the reaction rates and reaction durations were estimated using the experimental data with the uncoated particles such that the heat generation estimations are not over conservative.

Calculated heat generation rates were used as input parameter for the computational heat transfer model. The dissipation of the heat generated and the distribution of temperature were investigated for various conditions. Primarily, the temperature increase at depth of 0.5 cm from the wellbore was taken to be the focus of interest. For a heat generation rate of 325 kW/m^3, which is one-tenth of the uncoated particles' heat generation, and a replenishment time of 2 hours, the temperature increase at 0.5 cm depth is calculated to be around 160 °F. The analysis was done with lower heat generation rates while keeping all of the other parameters the same. Expectedly, the highest temperature increase at the same location is decreased not only due to lower heat generation but also due to circulation rate not being optimum for the new heat generation rate. It was seen that the circulation rate, the reaction time, and the heat generation rate are closely linked. The circulation rate must be optimized for the highest amount of heat generation to occur in the desired location. The effect of circulation rate was demonstrated by running the computational model with the same rate of heat generation and two different circulation rates. It was seen that there is more than 50 °F difference in the temperature increase at 0.5 cm depth from the sand face for the same amount of heat generation and different circulation rates.

The temperature increase was then used to calculate thermal stresses for different rock properties. It is noteworthy that the thermo-elastic properties of the rocks are of crucial importance for thermal stress calculations and that there is a wide range of

material properties. Depending on the application zone, there might be very large differences in thermal stress for the same amount of temperature increase.

5.2 FUTURE WORK

Future studies on this subject can be divided into three categories: (1) experimental methods, (2) improvements to the model, and (3) rock mechanics modeling.

The experiments conducted with the uncoated particles result in temperatures as high as 262 °F. It is important to verify that this temperature is not high enough to boil the brine. As expected dissolved salt in the water increases the boiling point of water but it is important to prove that this increase is more than 50 °F. One way to improve the experimental procedures is to conduct the experiments under high pressure. Special attention needs to be paid to pressure particularly to make sure that the high pressure does not affect the reaction kinetics.

There are several improvements that can be made in terms of modeling. The developed method is comprehensive enough to model many aspects of the heat transfer phenomenon, and the model can be made more robust. Some problem parameters such as heat transfer coefficients depend on other problem parameters such as flow conditions or cross sectional geometry. Various heat transfer correlations can be embedded in the model so that the heat transfer coefficients are automatically calculated rather than users choosing them themselves.

In terms of thermal stress calculation, a more complex model (e.g. from a commercial software package) can be utilized along with the thermal model by mapping the transient temperature distributions obtained from the thermal model. The analytical solutions for thermal stress calculations may not be accurate for complex models such as this, although they are good as starting points. Along with the thermal stress calculation,

thermal expansion of the rock should be investigated in order to understand the behavior of porous media. For fracture gradient calculation, the implications of significant temperature increase on parameters other than the thermal stress such as pore pressure should be studied.

Appendix A: Line Gauss Seidel Iterative Method

In this section, the Line Gauss Seidel Method, which was used to solve the linear system, is explained.

A.1 TRI-DIAGONAL MATRIX ALGORITHM (TDMA)

Tri-diagonal Matrix algorithm is a direct method to solve 1D linear systems for which the coefficient matrix is a sparse matrix with only diagonal and one-off diagonal elements as in Figure A.1-1, since each node has two neighbors in 1D.

$$\begin{bmatrix} x & x & & & & \\ x & x & x & & & \\ & x & x & x & & \\ & & x & x & x & \\ & & & x & x & x \\ & & & & x & x \end{bmatrix}$$

Figure A-1: Structure of coefficient matrix for 1D problems

For an arbitrary point, i, the form of the equation is shown in equation A.1.

$$a_i\phi_i = b_i\phi_{i+1} + c_i\phi_{i-1} + d_i \tag{A.1}$$

For boundary points $c_1 = 0, b_N = 0$, since there is only one neighboring point. The equation for the first grid point can be used to write $\phi_1 = f(\phi_2)$. Substituting this expression into the equation for the second point helps eliminating $\phi_1$to get $\phi_2 = f(\phi_3)$. The process is repeated until the very last point to obtain ϕ_N. Then ϕ_N is used to calculate the rest of the unknown values by back substitution. The method is equivalent to Gaussian elimination which is a direct solution method. The method is formalized in the following way:

$$\phi_i = P_i \phi_{i+1} + Q_i \tag{A.2}$$

The coefficients P and Q are defined to satisfy equation A.2. Equation A.2 and equation A.1 gives the following formulation for each grid point:

$$P_i = \frac{b_i}{a_i - c_i P_{i-1}} \tag{A.3}$$

$$Q_i = \frac{d_i + c_i Q_{i-1}}{a_i - c_i P_{i-1}} \tag{A.4}$$

The boundary values for P and Q are $P_1 = b_1/a_1$, $P_N = 0$, and $\phi_N = Q_N$.

Using equations A.3 and A.4, P and Q values are calculated in the forward sweep until the Q values are calculated for the last grid point, which is equal to the unknown value for that grid point. Then, with a backward sweep, the rest of the unknown values are calculated using equation A.2 for which, at each step, the only unknown is the left-hand-side value.

A.2 LINE BY LINE TDMA

TDMA is a direct method to solve one-dimensional problems. For multi-dimensional problems, an iterative method called line by line TDMA or Line Gauss Seidel is developed based on TDMA. The Line Gauss Seidel method requires structured meshes. TDMA method is applied along a line assuming that the values on either side of the line are temporarily known. The process is repeated on each line by sweeping across the entire domain, and by updating the values of each line until the convergence is achieved. For each grid point the equation A.5 can be written, relating each node to 4 neighbors in two-dimensional problems.

$$a_{ij}\phi_{ij} = b_{ij}\phi_{ij+1} + c_{ij}\phi_{ij-1} + g_{ij} + d_{ij}\phi^*_{i+1j} + e_{ij}\phi^*_{i-1j} \tag{A.5}$$

In Figure A-2, the procedure for line by line TDMA is depicted. The sweep the direction is chosen to be i, whereas TDMA is solved along each line in j direction. The equation A.5 is written to solve TDMA for an arbitrary line, i. The values denoted with $*$ in equation A.5 are neighboring lines which are assumed to be known temporarily.

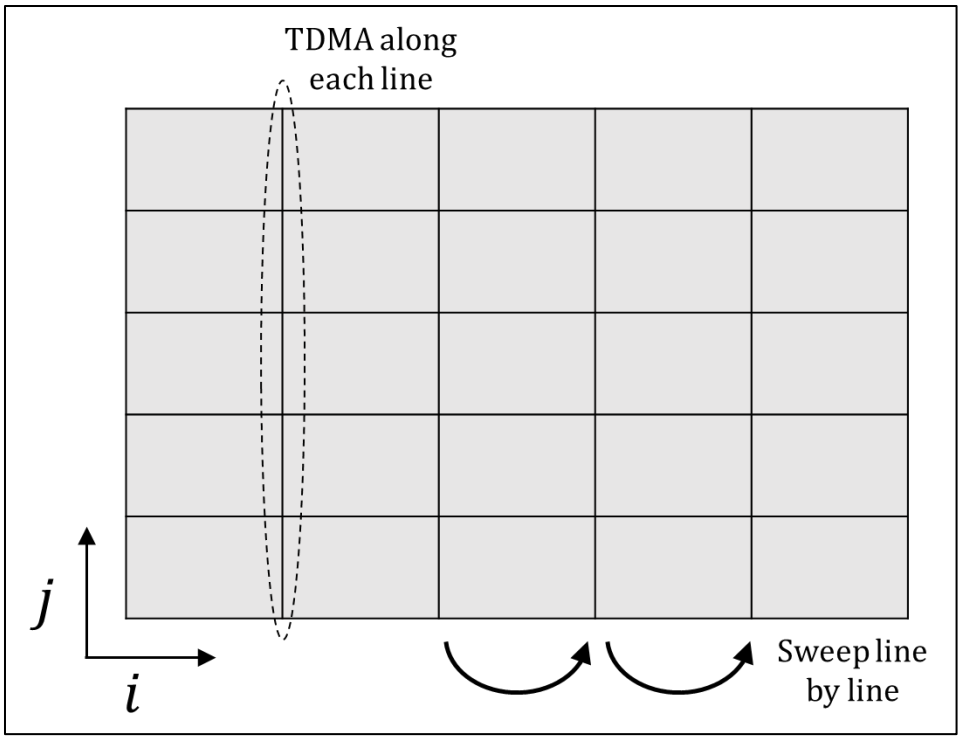

Figure A-2: Line by line TDMA procedure

Appendix B: Solutions of the Hasan and Kabir Method

Equation 3.15 is a second-order, inhomogeneous linear differential equation. It is possible to write it in the following way to separate out the inhomogeneous term.

$$AB\frac{d^2T_t}{dz^2} + B\frac{dT_t}{dz} - T_t = -T_{es} - g_G z = f(z) \tag{B.1}$$

In order to obtain the particular solution of B.1, a solution can be assumed in polynomial form and the coefficients can be calculated by substitution of the assumed solution into B.1.

$$T_{tp} = C_1 z + C_2 \tag{B.2}$$

Substituting B.2 into B.1 gives:

$$BC_1 - C_1 z - C_2 = -T_{es} - g_G z \tag{B.3}$$

Equating the coefficients of z and the constant terms,

$$C_1 = g_G, C_2 = T_{es} + Bg_G \tag{B.4}$$

Therefore, the particular solution is found to be:

$$T_{tp} = g_G z + T_{es} + Bg_G \tag{B.5}$$

The homogeneous solution of B.1 is found by equating $f(z) = 0$.

$$AB\frac{d^2T_t}{dz^2} + B\frac{dT_t}{dz} - T_t = 0 \tag{B.6}$$

The characteristic equation,

$$AB\lambda^2 + B\lambda - 1 = 0 \tag{B.7}$$

$$\lambda_{1,2} = -\frac{1}{2A} \pm \frac{1}{2A}\sqrt{1 + \frac{4A}{B}} \tag{B.8}$$

The complementary solution to B.1 is

$$T_{tc} = \alpha e^{\lambda_1 z} + \beta e^{\lambda_2 z} \tag{B.9}$$

The complete solution is the sum of particular and complementary solutions.

$$T_t = \alpha e^{\lambda_1 z} + \beta e^{\lambda_2 z} + g_G z + T_{es} + B g_G \tag{B.7}$$

The annular fluid temperature can now be found by combining equations 3.13 and B.7.

$$\frac{dT_t}{dz} = \alpha\lambda_1 e^{\lambda_1 z} + \beta\lambda_2 e^{\lambda_2 z} + g_G \tag{B.8}$$

$$T_a = T_t - B\frac{dT_t}{dz} = (1 - \lambda_1 B)\alpha e^{\lambda_1 z} + (1 - \lambda_2 B)\beta e^{\lambda_2 z} + g_G z + T_{es} \tag{B.9}$$

In order to obtain α and β coefficients, boundary conditions are applied:

$$\left.\frac{dT_t}{dz}\right|_L = 0 = \alpha\lambda_1 e^{\lambda_1 L} + \beta\lambda_2 e^{\lambda_2 L} + g_G \tag{B.8}$$

$$T_a(0) = T_{as} = (1 - \lambda_1 B)\alpha + (1 - \lambda_2 B)\beta + T_{es} \tag{B.9}$$

$$\alpha = \frac{(T_{as} - T_{es})\lambda_2 e^{\lambda_2 L} + g_G(1 - \lambda_2 B)}{\lambda_1 e^{\lambda_1 L}(1 - \lambda_2 B) - \lambda_2 e^{\lambda_2 L}(1 - \lambda_1 B)} \tag{B.10}$$

$$\beta = \frac{(T_{as} - T_{es})\lambda_1 e^{\lambda_1 L} + g_G(1 - \lambda_1 B)}{\lambda_1 e^{\lambda_1 L}(1 - \lambda_2 B) - \lambda_2 e^{\lambda_2 L}(1 - \lambda_1 B)} \tag{B.11}$$

A similar analysis can be done to obtain the coefficients for conventional circulation.

$$\gamma = -\frac{(T_{ti} + Bg_G - T_{es})\,\xi_2 e^{\xi_2 L} + g_G}{\xi_1 e^{\xi_1 L} - \xi_2 e^{\xi_2 L}} \tag{B.12}$$

$$\delta = -\frac{(T_{ti} + Bg_G - T_{es})\,\xi_1 e^{\xi_1 L} + g_G}{\xi_1 e^{\xi_1 L} - \xi_2 e^{\xi_2 L}} \tag{B.13}$$

$$\xi_{1,2} = -\frac{1}{2A} \pm \frac{1}{2A}\sqrt{1 + \frac{4A}{B}} \tag{B.14}$$

Bibliography

Aadnoy, B.S. 1999. Optimization of mud temperature and fluid models in offshore applications. Offshore Europe Oil and Gas Exhibition and Conference. Aberdeen, United Kingdom, September 7.

Abdelkadeer, K.M., Senturk, E., Dunn-Norman, S., Goodman, H.E., Prada, M., and Rivera N. 2009. Changes in Near Wellbore Stress and Fracture Gradient Due to Cold Water Injection in a Sirte Basin Field, Libya. SPE/EAGE Reservoir Characterization and Simulation Conference, Abu Dhabi, UAE, October 19-21.

Adachi, J., Bailey, L., Houwen, O.H., Meeten, G.H., and Way, P.W. 2004. SPE/IADC Drilling Conference, Dallas, Texas, March 2-4.

Aktan, T., and Farouq Ali, S.M. 1976. Finite Element Analysis of Temperature and Thermal Stresses Induced by Hot Water Injection. SPE – AIME European Spring Meeting, Amsterdam, The Netherlands, April 8-9.

Ascencio-Cendejas, F., Reyes, O., and Nass, M.A. 2006. Thermal Design of Wells Producting Highly Viscous Oils in Offshore Fields in the Gulf of Mexico. First International Oil Conference and Exhibition in Mexico. Cancun, Mexico, August 31.

Bendiksen, K., Malnes, D., Moe, R., and Nuland S. 1992. The Dynamic Two-Fluid Model OLGA: Theory and Application. SPE Prod. Eng. May 1992, 171.

Bohun, C.S., McGee, B., and Ross, D. 2000. Electromagnetic Wellbore Heating. Fourth Annual Industrial Problem Solving Workshop, June 2000.

Brown, T.S., Clapham, J., Danielson, T.J., Harris, R.G., and Erickson, D.D. 1996. Application of a Transient Heat Transfer Model for Bundled, Multiphase Pipelines. SPE Annual Technical Conference and Exhibition. Denver, Colorado, October 6.

Calvert, D.G., and Griffin, T.J. 1998. Determination of Temperatures for Cementing in Wells Drilled in Deep Water. IADC/SPE Drilling Conference. Dallas, Texas, March 3.

Chin, Y.D., Perera, R., Prescott, C.N, and Cain, R.E. 2000. Thermal Performance of an Insulated Multiple Flowline Bundle Using Active Heating. SPE International Petroleum Conference and Exhibition in Mexico. Villahermosa, Mexico, February 1.

Circ. PS-2018, *Report of Meeting of API Committee 10.* 1993 API Standardization Conference. August 1993, New Orleans, Louisiana.

Closmann, P.J., and Phocas, D.M. 1976. SPE – AIME 51st Annual Fall Technical Conference and Exhibition, New Orleans, Louisiana, October 3-6.

Duret, E., Lebreton, E., Heintze, E. Henriot, V., and Saint-Marcoux, J.F. 2000. Pipeline Bundles Model Implemented Into a Multiphase Flow Model. SPE Annual Technical Conference and Exhibition. Dallas, Texas, October 1.

Edwardson, M.J., Girner, H.M., Parkison, H.R., Williams, C.D., and Matthews, C.S. 1962. Calculation of Formation Temperature Disturbances Caused by Mud Circulation. *SPE Journal of Petroleum Technology* **14**(4): 416-426.

Enayatpour, S., and Patzek, T. 2013. Thermal Shock in Reservoir Rock Enhances the Hydraulic Fracturing of Gas Shales. Unconventional Resources Technology Conference, Denver, Colorado, August 12-14.

Feng, M. 2011. The Temperature Prediction in Deepwater Drilling of Vertical Well. Dissertation, Texas A&M University.

Hasan, A.R., and Kabir, C.S. 1996. A Mechanistic Model for Computing Fluid Temperature Profiles in Gas-lift Wells. *SPE Production & Operations* **11**(3) 179-185.

Holmes, C.S., and Swift, S.C. 1970. Calculation of Circulating Mud Temperatures. *SPE Journal of Petroleum Technology* **22**(6): 670-674.

Imran, T.N.O.M., Al Izudin, A., Natasha, M.S., Samsudin, N., Rameli, M.F., Hamid. A.A.A., Elliott, C., Khalid, M.Z., and Zeidan, A.A., 2010. Challenges in Designing, Planning and Execution of Well Completions for Highly Depleted Reservoirs, and High Differential Pressure Between Reservoirs. SPE Asia Pacific Oil and Gas Conference and Exhibition, Brisbane, Queensland, Australia, October 18-20.

Incropera, Frank P, and Frank P Incropera. 2007. Fundamentals Of Heat And Mass Transfer. Hoboken, NJ: John Wiley.

Izgec, B., Hasan, A.R., Lin, D., and Kabir, C.S. 2010. Flow-Rate Estimation From Wellhead-Pressure and Temperature Data. *SPE Production &Operations* **25**(1): 31-39

Kabir, C.S., Hasan A.R., Kouba, G.E., and Ameen, M. 1996. Determining Circulation Fluid Temperature in Drilling, Workover, and Well Control Operations. *SPE*

Drilling & Completion **11**(2): 74-79.

Kartevoll, M. 2009. Drilling problems in depleted reservoirs. Thesis, Universitetet i Stavanger.

Marshall, T.R., and Lie, O.H. 1992. A Thermal Transient Model of Circulation Wells: 1. Model Development. European Petroleum Computer Conference. Stavanger, Norway, May 24.

Maury, V., and Idelovici, J.L. 1995. Safe Drilling of HP/HT Wells, The Role of the Thermal Regime in Loss and Gain Phenomenon. SPE/IADC Drilling Conference, Amsterdam, The Netherlands, February 28 – March 2.

Mehta, A.P., Zabaras, G.J., Schoppa, W., and Peters, D.J. 2004. Unlocking Deepwater Heavy Oil Reserves: A Flow Assurance Perspective. Offshore Technology Conference. Houston, Texas, May 3-6.

Mills, Anthony F. 1999. Heat Transfer. Upper Saddle River, New Jersey: Prentice Hall.

Minkowycz, W. J., Sparrow, E.M., and Murthy, J.Y. 2006. Handbook Of Numerical Heat Transfer. Hoboken, New Jersey: Wiley.

Parman, D.G., O'Brien, K., and Farzaneh, F. 2014. Downhole Wellbore Heating System and Method. U.S. Patent 2014/0099084 A1, filed September 20, 2013, and issued April 10, 2014.

Patankar, Suhas V. 1980. Numerical Heat Transfer And Fluid Flow. Washington: Hemisphere Pub. Corp.

Perkins, T.K., and Gonzalez, J.A. 1981. Changes in Earth Stresses Around a Wellbore Caused by Radially Symmetrical Pressure and Temperature Gradients. SPE Annual Technical Conference and Exhibition, San Antonio, Texas, October 5-7.

Piber, M., Prohaska, M., Hublik, G., and Thonhauser, G. 2006. Time-Dependent Behavior of Drilling Fluids Under Cyclic Temperature and Pressure Loads. SPE Annual Technical Conference and Exhibition. San Antonio, Texas, September 24.

Press, W.H., Teukolsky, S.A., Vetterling, W.T., and Flannary, B.P. 1992. Numerical Recipes in FORTRAN: The Art of Scientific Computing, Cambridge University Press.

Ramey JR., H.J. 1962. Wellbore Heat Transmission. *SPE Journal of Petroleum Technology* **14**(4): 427-435

Raymond, L.R. 1969. Temperature Distribution in a Circulation Drilling Fluid. *SPE*

Journal of Petroleum Technology **21**(3): 333-341.

Schoeppel, R.J., and Bennett, R.E. 1971. Numerical Simulation of Borehole and Formation Temperature Distributions While Drilling to Total Depth. Fall Meeting of the *Society of Petroleum Engineers of AIME.* New Orleans, Louisiana, October 3.

Stiles, D., and Trigg, M.J. 2007. Mathematical Temperature Simulators for Drilling Deepwater HTHP Wells: Comparisons, Applications, and Limitations. SPE/IADC Drilling Conference. Amsterdam, The Netherlands, February 20.

Tahmourpour, F., and Quinton, C.W. 2009. Saving Expensive Offshore Deepwater Rig Time by Modeling Accurate Subsea/Subsea Floor Temperature Modeling for Cementing Operations. SPE Annual Technical Conference and Exhibition. New Orleans, Louisiana, October 4.

Tang, L., and Luo, P. 1998. The Effect of the Thermal Stress on Wellbore Stability. SPE India Oil and Gas Conference and Exhibition. New Delhi, India, February 17-19.

Wooley, G.R. 1980. Computing Downhole Temperatures in Circulation, Injection, and Production Wells. *SPE Journal of Petroleum Technology* **32**(9): 1509-1522.

Yang, M., Meng, Y., Li, G., Li, Y., Chen, Y., Zhao, X., and Li, H. 2013. Estimation of Wellbore and Formation Temperatures During the Drilling Process under Lost Circulation Conditions. *Mathematical Problems in Engineering, 2013.*

Zabaras, G.J., and Zhang, J. 1997. Steady-state and Transient Thermal Performance of Subsea Hardware. Offshore Technology Conference, Houston, Texas, May 5-8.

Zazovsky, A.F., Haddad, S., and Tertychnyi, V. 2005. Thermal History Reconstruction and Estimation of Formation Temperature Using Wireline Formation Tester Measurements. SPE Europec/EAGE Annual Conference. Madrid, Spain, June 13.

Zoback, M.D., Barton, C.A., Brudy, M., Castillo, D.A., Finkbeiner, T., Grollimund, B.R., Moos, D.B., Peska, P., Ward, C.D., and Wiprut, D.J. 2003. Determination Of Stress Orientation And Magnitude In Deep Wells. *International Journal Of Rock Mechanics And Mining Sciences* **40**(7-8): 1049-1076.